Polymer Testing 128 (2023) 108246

Contents lists available at ScienceDirect

Polymer Testing

journal homepage: www.elsevier.com/locate/polytest

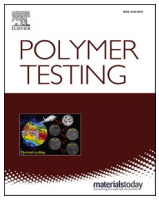

# Biaxial experimental characterizations of soft polymers: A review

Ali Esmaeili, Deepak George, Ian Masters, Mokarram Hossain *

*Zienkiewicz Institute for Modelling, Data and AI, Faculty of Science and Engineering, Swansea University, SA1 8EN, United Kingdom*

ARTICLE INFO

*Keywords:*
Elastomeric polymers
Hydrogels
Biaxial test
Digital image correlation
Cruciform geometry
Sample optimization

ABSTRACT

Soft polymeric materials such as elastomers and hydrogels have played a significant role in recent interdisciplinary research. They are subjected to large stretch and high cyclic loading-unloading conditions where the typical loading mode is biaxial rather than simple uniaxial loading, thus, necessitating further characterization using biaxial loading conditions and subsequently developing robust and versatile numerical models. Although many standards were prepared for common uniaxial tests in situ elastomers including tensile, shear, and fatigue tests, no specific standardized guidelines were prepared to be employed for the biaxial characterization of elastomers and hydrogels. There existed limited works on the biaxial characterization of soft polymers, thus, making it difficult to identify which configurations and results are more reliable. Hence, there were huge discrepancies in the existing literature for biaxial tests in terms of sample configurations (square or cruciform specimens), dimensions, and test setups including strain rate, pre-loading, equi-biaxial and unequi-biaxial tests. Therefore, this paper is aimed at reviewing the published studies on the biaxial characterization of soft polymers in several aspects including (i) sample configurations in terms of geometry and dimension (ii) biaxiality degree of tested specimens where sample should be optimized to reach proper biaxiality, i.e., larger area with homogenous strain distribution in the middle with respect to the edges, (iii) test procedure for the biaxial characterization including strain amplitude, strain rate and loading patterns (iv) a brief review on inflation test of elastomers which was the most common equi-biaxial test studied in the literature. The largest and smallest cruciform samples with the dimensions of $165 \times 165$ mm$^2$ and $38 \times 38$ mm$^2$ were used, respectively, while a small sample of $7 \times 7$ mm$^2$ and large one of $70 \times 70$ mm$^2$ were also employed for the square specimen. It was concluded that various test parameters and materials were used for the biaxial characterization. This necessitates the importance of preparing a standardized methodology for the biaxial characterization of elastomers based on intended materials and applications. Hence, a few potential geometries based on the optimization performed in the literature were suggested for future investigations in which numerous examinations using different materials and test parameters shall be conducted to reach an ideal sample configuration and methodology for the biaxial characterization of soft polymeric materials.

## 1. Introduction

Elastomers, thermosets, and thermoplastics are three main types of polymers that are composed of polymerization of a subunit called monomer. Elastomeric materials such as rubbers, silicones, hydrogels have been widely used in many applications including vibrations and shock absorbers [1,2], tires [3,4], sealing and sound proofing systems [5,6], wave energy harvesting [7–11], flexible electronics i.e. wearable technologies [12,13] tissue engineering [14,15] and soft robotics [16–18]. Soft materials are defined as any materials with Young's modulus in the range of $10^3$–$10^9$ Pa [19] as shown in Fig. 1a. The term soft polymers, hereinafter, refer to elastomers including rubbers, silicones (e.g.VHB, eco-flex), and hydrogels which possessed hyperelastic and viscoelastic behaviours. It should be noted that human tissues such as skins, cartilages and tendons are not the scope of this paper. Nevertheless, the outcome of this paper can be beneficial for them as performing biaxial test for soft tissues exhibiting anisotropic and viscoelastic behaviours is crucial [20–26].

One of the main characteristics of elastomeric materials is their ability to undergo large strain, known as hyperelasticity. Hyperelastic materials usually demonstrate nonlinear stress-strain behaviour where they are also subjected to high cyclic loading(e.g.,uniaxial and biaxial), during their service life resulted in more susceptibilities to fatigue failure [27].There has been significant research into mechanical behaviour

* Corresponding author.
*E-mail address:* mokarram.hossain@swansea.ac.uk (M. Hossain).

https://doi.org/10.1016/j.polymertesting.2023.108246
Received 3 August 2023; Received in revised form 5 October 2023; Accepted 19 October 2023
Available online 21 October 2023

of elastomers over the last few decades [28–32]. The most typical mechanical tests conducted on soft polymers are compression [33–37], tension [38–40], tear [41,42] and shear tests [43–47] which were mainly performed in simple loading conditions i.e. uniaxial mode. In contrast, fewer works were done in biaxial loading (Fig. 1b). Although a combination of dynamic loading conditions i.e. shear and compression modes are typical loading scenarios for tire applications, many other areas such as the flexible membranes employed in wave energy convertor devices and soft robotics requires a good dynamic mechanical property in the biaxial modes [7]. Therefore, when considering the service condition of elastomers that are subject to complex and alternating loading scenarios, obtaining material characteristics from both quasi-static and dynamic biaxial tests are essential.

High fidelity mathematical modelling of elastomers is an active research field. To develop accurate constitutive models of these materials, numerous strain energy functions both for isotropic and anisotropic elastomers have been used to better understand the deformation of hyperelastic materials including Neo-Hookean [48], Mooney-Rivlin [49,50], Yeoh [51], Ogden [52], limiting chain extensibility models [53,54], and finally comprehensive model developed by Anssari [55]. Extensive reviews of these models can be found in Hossain et al. [56–58]. Nevertheless, reliable and accurate material parameters appearing in a hyperelastic model cannot be easily obtained using experimental data obtained from uniaxial tests. Hence, it is necessary to perform both uniaxial and biaxial tests to achieve more precise models [59–61].

Bulge test, also known as the inflation test, is the most common type of biaxial test conducted on elastomers and thin films (Fig. 1b). However, thickness variations throughout the membrane during pressurisation result in severe nonlinear mechanical behaviour i.e. inhomogeneous stress and strain distributions, in particular at large strain amplitudes so that the developed outcomes cannot be reliable [62,63]. Therefore, other test configurations for the biaxial characterization using square and cruciform samples will also be investigated throughout this review in addition to the classical bulge (inflation) test. A literature review shows that there have been different configurations for biaxial tests including square and cruciform geometries with different dimensions. Axel Products *Inc* developed a rig to test elastomers in

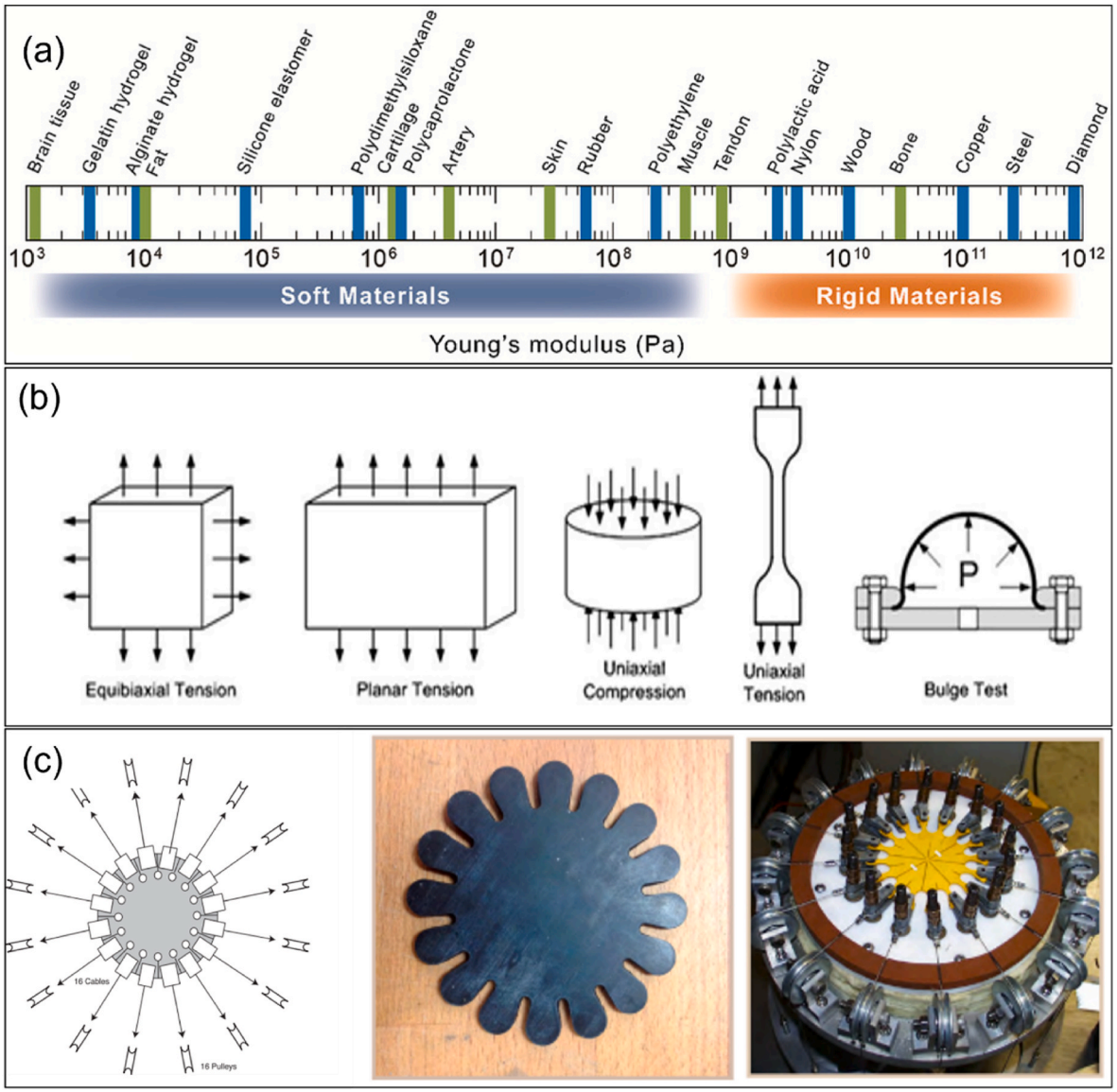


**Fig. 1.** (a) Soft and rigid materials definition [19], *(b) few most common mechanical tests performed on rubber-like materials, i.e. equi-biaxial tension, planar tension, uniaxial compression/tension, and bulge test mimicking axisymmetric loading condition* [67], *(c) a disk-shaped sample stretched radially using 16 grips developed by Axel Products Inc* [61,64].

equibiaxial mode using a circular specimen which is radially stretched by 16 arms evenly distributed on its circumference [64,65]. These variations in experimental procedures make it difficult to interpret the existing experimental data. Published works on the biaxial characterization of soft elastomers have been varied in different aspects that can be summarized as follows: (i) sample dimension in terms of geometry (cruciform/square) and dimension (ii) sample optimization in the case of a better biaxiality degree, (iii) test procedure for biaxial characterization including strain amplitude, strain rate, applied load patters, gripping system (iv) the issues related to the inflation test of elastomers which is the most common biaxial test studied in the literature. Note that it is of importance to achieve homogenous strain distribution within the area of interest during the biaxial characterization. In addition, biaxial test conditions of largely stretchable elastomeric materials are severely dependent on the clamping systems used, necessitating proper design and probably reinforcement of the clamping regions [66].To the best of authors' knowledge, there is no existing review work that can portray a clear picture on the biaxial experimental characterization of soft polymers considering all the aforementioned aspects. Hence, the current review will fill the gaps existing in the literature. In this context, a brief review of various sample geometries used in biaxial mode is performed in section 2 while the definition of proper biaxiality and subsequently sample optimization are thoroughly discussed in section 3. A summary of the available biaxial test methodologies for elastomers and hydrogels in the aspect of hyper-viscoelastic and fracture characterizations are conducted in section 4 followed by a short review of the bulge test throughout section 5. The necessity of preparing a standardized procedure for biaxial characterization are discussed in section 6 in which a few potential geometries and test setups in addition to specimen reinforcement are suggested for future characterizations.

## 2. Sample configuration

Up to now, no specific standard has been proposed to clarify how the biaxial specimen should be prepared in terms of its configuration and geometry. Hence, various specimen geometries have been used including cruciform (of various sizes and shapes) as well as square samples. Fig. 2 shows some commonly used geometries for biaxial characterization including cruciform and square geometries. It is clear from the figures that there is a high degree of discrepancy amongst published works in terms of sample shapes and dimensions. Indeed, the largest and the smallest cruciform samples with the dimensions of 165 ×

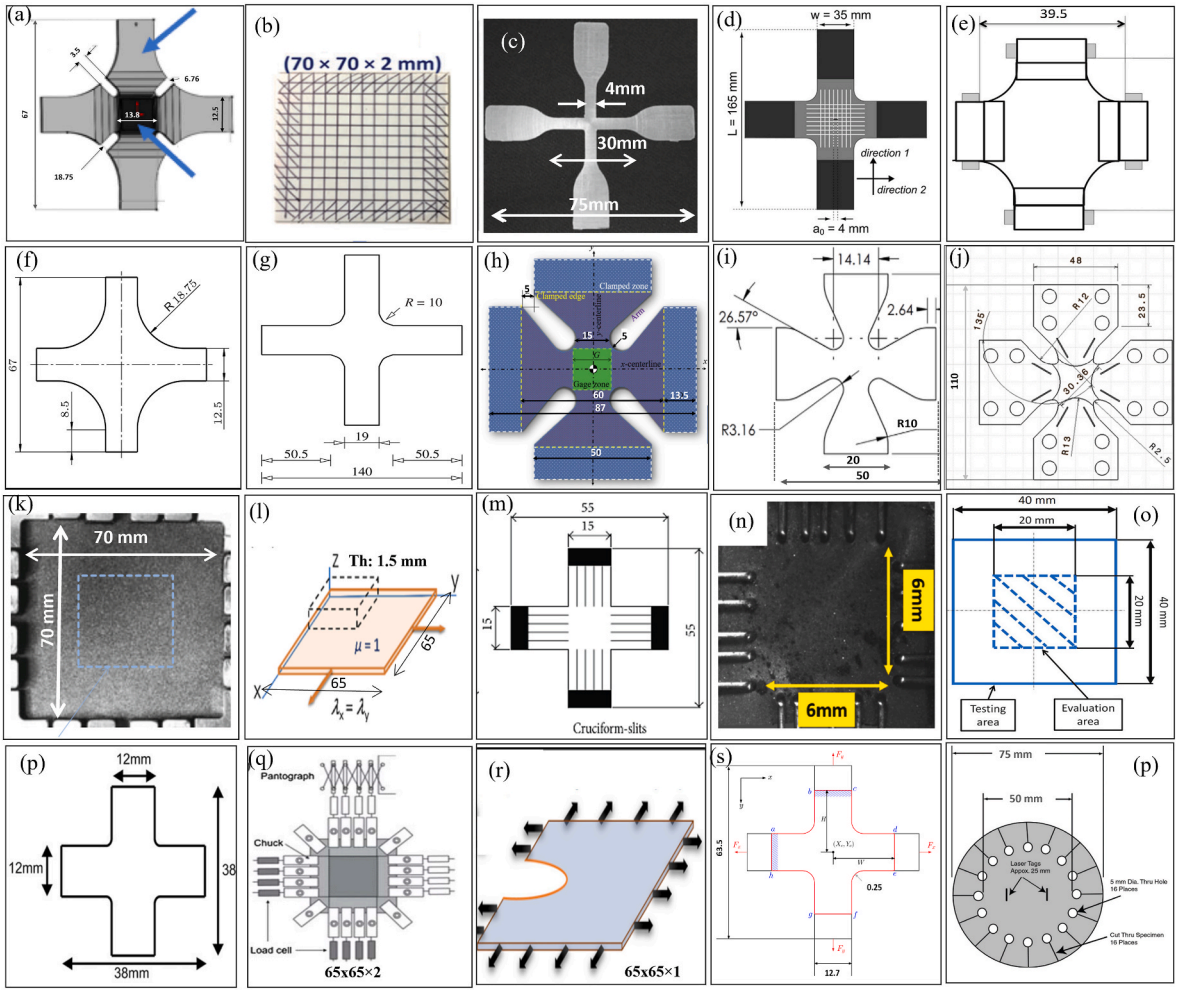


**Fig. 2.** Sample configurations for biaxial characterization with a wide range of soft polymeric materials: (a) 3D printed sample made of TangoBlackPlus [68], *(b) SBR filled with silica prepared using a Brabender-type mixer* [69], *(c) ELASTOSIL® RT 265 produced by casting* [70], *(d) NR filled with carbon black made by compression moulding* [71], *(e) NR filled with carbon black* [72], *(f) elastomeric material* [73], *(g) PP/PE,Polypropylene/polyethylene, biaxial sample* [74], *(h) 3D printed silicon rubber* [75], *(i) magnetorheological elastomers (MRE) prepared by casting* [76], *(j) poly(ethylene terephthalate) (PET) prepared by injection moulding* [77], *(k) styrene butadiene rubber (SSBR) filled with carbon black* [78], *(l) double network hydrogels* [79], *(m) rubber like samples cut from a sheet* [80], *(n) latex, oppo band and ecoflex cut from a sheet* [81], *(o)* polyvinylidene difluoride (PVDF) flat membrane [82], (p) n*afion membranes* [83], *(q) chemically and physically cross-linked hydrogels* [84], *(r) hydrogel* [85], *(s) NR filled with CNT* [86], *(p) elastomeric disk-shaped specimen* [64]. (For interpretation of the references to colour in this figure legend, the reader is referred to the Web version of this article.)

165 mm$^2$ (Figs. 2d) and 38 × 38 mm$^2$ (Fig. 2p) were used, respectively, while a small sample of 7 × 7 mm$^2$ (Fig. 2n) and large one of 70 × 70 mm$^2$ (Fig. 2k) were also used for the square specimen. It is quite difficult to indicate which configuration is ideal for the biaxial characterization since different materials and loading conditions were employed. This necessitates the importance of developing a standardized procedure for biaxial characterization of various soft materials. This can be also of particular interest for studying physiology and anisotropic behaviour of human tissues in which performing a reliable biaxial test in vitro is quite challenging due to boundary conditions i.e. stress concentration imposed to the sample from the grips as well as varied sample geometries used [20–24].

Apart from the cruciform and square samples, a circular specimen with diameter of 75 mm was equi-biaxially tested at *Axel Products Inc* [64]. in which it was claimed their test methodology can also be used instead of simple uniaxial compression for incompressible materials such as rubbers (Fig. 2p). This was attributed to the detrimental effect of friction during simple uniaxial compression. They have employed a series of experimental tests to verify hyperelastic models for elastomers including uniaxial tension, planar tension, and equal biaxial extension. Radial slits were created into the sample to separate the grips while the holes were introduced to avoid premature failure in the vicinity of the grips.

## 3. Sample optimization and biaxiality degree

One of the main challenges in running biaxial test is to achieve homogeneous strain and stress distributions in the field of interests, typically in the middle of the samples (both cruciform and square specimens) [87–93]. However, it is hard to achieve due to the gripping effect which causes stress concentration near the edge arisen from the grips [66] along with a wider area of the middle (for the cruciform sample) which decreases the stress in the middle (Fig. 3a). Therefore, some studies discussed sample optimization for a better biaxiality degree and a homogenous strain distribution within the cruciform specimen. For instance, Seibert et al. [73] investigated the effect of various cruciform geometries as shown in Fig. 3b. As it is shown in Fig. 3a, samples are varied in terms of the fillet radius, width and length of the arm, which are indispensable geometric properties. However, the dimensions of the clamping region and overall dimension of the specimen were kept constant.

For that, a set of criteria was defined leading to a perfect biaxially state including:

$$\Gamma(x,y) = \left| E_{xx}^{(x,y)} - E_{yy}^{(x,y)} \right| \tag{1}$$

$$\eta = \frac{E_{xx}^{c}}{E_{xx}^{max}} \quad if\ E_{xx}^{c} = 0.1 \rightarrow \eta^{(0.1)} = \frac{0.1}{E_{xx}^{max}} \tag{2}$$

$$Q^{(0.1)} = \frac{\eta^{(0.1)}}{100 \times \sigma_{\Gamma}^{c}} \tag{3}$$

in which $E_{xx}^{(x,y)}$ *and* $E_{yy}^{(x,y)}$ are principal strains in x and y directions, respectively, $\Gamma(x,y)$ test function, $\eta$ degree of efficiency, $\eta^{(0.1)}$ scaled degree of efficiency, $\sigma_{\Gamma}^{c}$ standard deviation of the test function, $Q^{(0.1)}$ quality factor. It is worth noting that a perfect biaxiality means that the principal strains in the center of the sample, $E_{xx}^{c}$ and $E_{yy}^{c}$ , should be equal, thus, test function $\Gamma(x,y)$ (equation (1)) indicates the variations from perfect biaxiality in the region of interest, i.e., the more $\Gamma(x,y)$ the more uniaxiality and vice versa. The test function over the horizontal axis (the distance AB shown by white dashed arrows in Fig. 3a)is shown in Fig. 3c where type A and D configurations manifest better biaxiality compared to type B and C.

Apart from the perfect biaxiality, the uniaxial strain within the arms is much higher than the middle area i.e. $E_{xx}^{(x,y)} \gg E_{xx}^{c}$ and $E_{yy}^{(x,y)} \gg E_{yy}^{c}$ , thus, a new factor was taken into account to define the Degree of Efficiency (DOE) (equation (2)). This demonstrates the strain discrepancy between the arm and the center region in which a DOE of 0.25, 0.12, 0.09, and 0.29 were achieved for type A to D, respectively. Therefore, type B and C geometries cannot be ideal configurations resulting from their high-test functions and low DOEs. Finally, a combination of both test function and

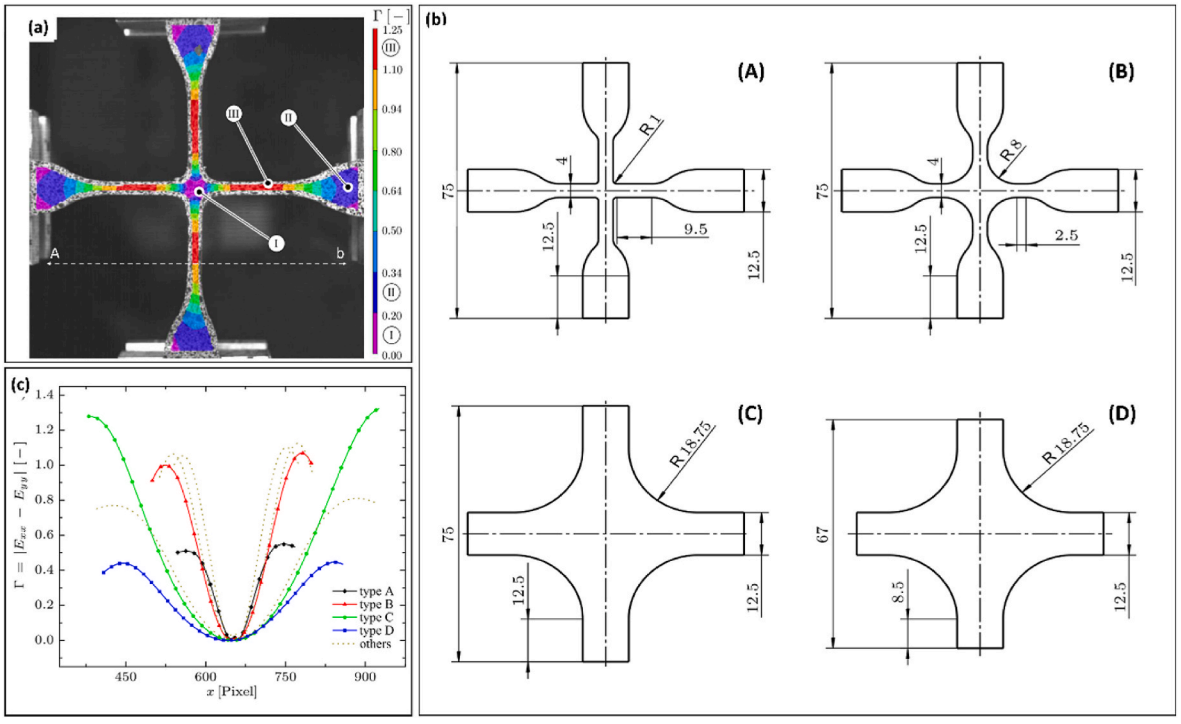


**Fig. 3.** (a) High strain near the gripping region as well as the arm, (b) different sample geometries, (c) test functions within one arm of the cruciform sample refer to distance AB illustrated in (a) [73].

DOE was considered to identify an optimum sample for perfect biaxiality led to the definition of the quality factor (equation (3)). Type A manifested a quality factor of 0.04 whereas type D represented a value of 1.03. The low quality factor for the type A was attributed to high standard deviation within the sample with respect to the type D. It was concluded that type D shows better performance in terms of a better degree of biaxiality.

Hartmann et al. [74] defined two important parameters for achieving proper biaxiality during a tension test of a cruciform specimen including formation of large strain and uniform strain distribution in the middle region; otherwise, a large strain can be observed in the arm as shown in Fig. 4a. It was noted that the arm should be stiffer compared to the middle area to achieve relatively large strain in the middle i.e., samples should be reinforced in the arm regions or moulded with thicker edges. This was done by gluing PP/PE (polypropylene/polyethylene) on both sides of the specimen with either square or circle-shape holes in the middle and with/without four cuts in the corners as shown in Fig. 4b. Therefore, several distinct geometries of the reinforced cruciform specimens along with the original shape (no reinforcement) were investigated to find out which configuration resulted in a larger strain and homogenous strain distribution in the middle area (Fig. 4a–c). The unreinforced specimen shows maximum strain in the arm rather than the middle (Fig. 4a). However, the reinforced specimens resulted in larger strains in the center as shown in Fig. 4b regardless of the configuration used. Equations (4) and (5) were defined to obtain the strain distribution within the center of the sample:

$$l_{m=}0.2\times l_0 \tag{4}$$

$$\varepsilon_{err=}\frac{|\varepsilon-\varepsilon_m|}{|\varepsilon_m|}\times 100 \tag{5}$$

where $l_0$ is the length of the smaller thickness region in the center, $l_m$ is the mean length of the central area, $\varepsilon_m$ is the mean strain value, and $\varepsilon_{err}$ is the relative error.

As it is shown in Fig. 4d, the effect of reinforced arm (shown in Fig. 4b) to reach homogeneous strain distribution in the middle is not fully practical i.e., a region of 0.5 $l_0$ manifested low error in the center whereas the other regions exhibited high deviations. Similarly, addition of different slots (Fig. 4c) to the reinforced specimen with a square hole in the middle, does not show significant change in reaching homogeneous strain distribution, although the one with slot distancing 4 mm from the middle square illustrates a better strain distribution (Fig. 4e). Finally, an epoxy moulded cruciform samples with thickness of 5 and 0.4 mm for the arm and centre, respectively, were tested for comparison in which no significant homogeneity was identified (Fig. 4f).

Modification of the shape of a 3D-printed cruciform samples made of silicone rubber subjected to biaxial tension test (with the stretch ratio of maximum $\lambda = 2$ in the center) was investigated by Putra et al. [75]. The aim of their experimental study was to identify material parameters of four commonly used hyperelastic models using a least square method. Five different geometries (by changing W and r, the narrowest width of the arm and fillet radius, respectively) were prepared as shown in Fig. 5a to find out the optimum shape of the sample in which a maximum stretch ($\lambda$) in the gauge area can be achieved. Equation (2) [73] was used to identify the degree of efficiency amongst various samples, denoted as $\eta$ in their study as illustrated in Fig. 5b. The maximum stretch was considered less than the stretch at failure in the uniaxial tensile test ($\lambda_{UTS} < 4$) to guarantee no failure takes place during the biaxial test. Finally, Finite Element Method (FEM) was employed to identify the optimum shape in which the maximum elongation can be achieved in the middle rather than in the arm. It was concluded that geometry #4 i.

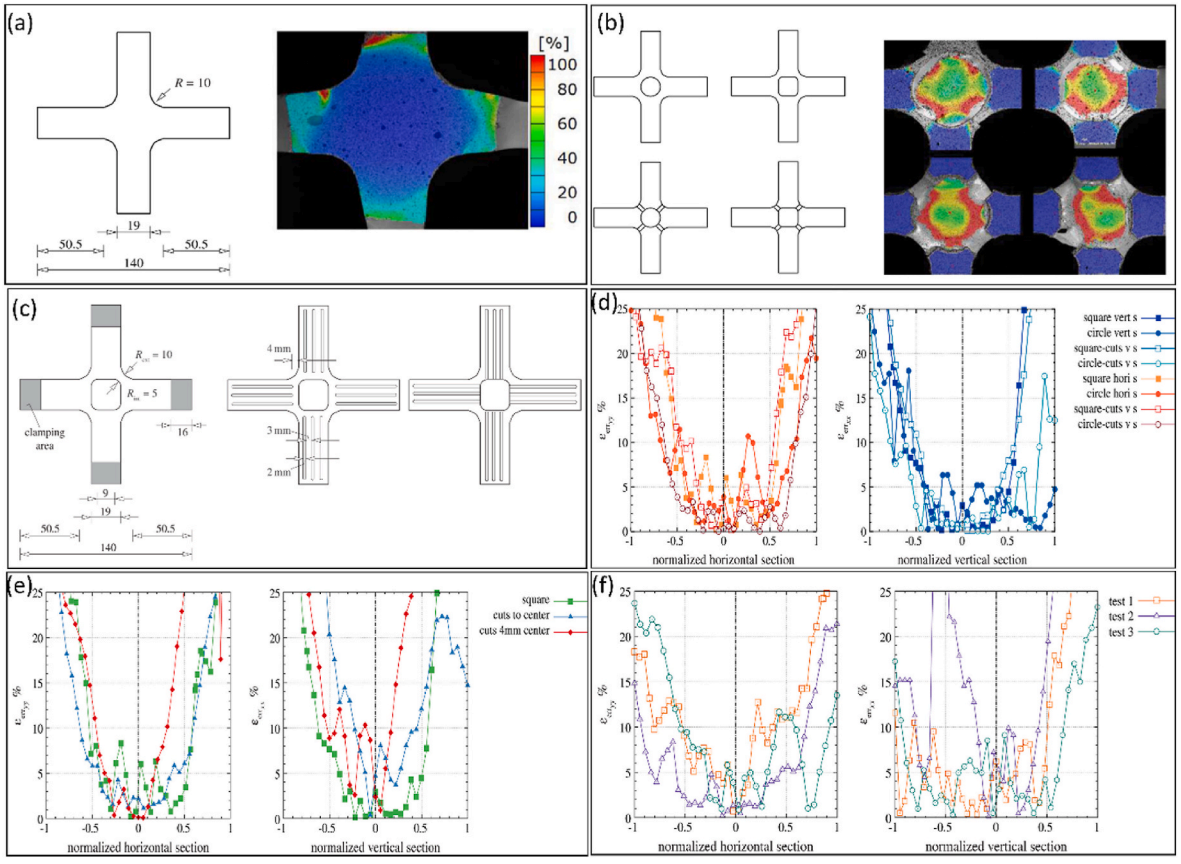


**Fig. 4.** Comparison of strain distribution in varied geometries: (a) unreinforced cruciform specimen, (b) different reinforced specimens with a square or circle hole in the middle, (c) reinforced samples with two different slots within the arm,(d–e) strain distribution versus normalized length corresponding to designed shapes shown in.b-c, respectively, (f) strain distribution versus normalized length for moulded-epoxy specimen [74].

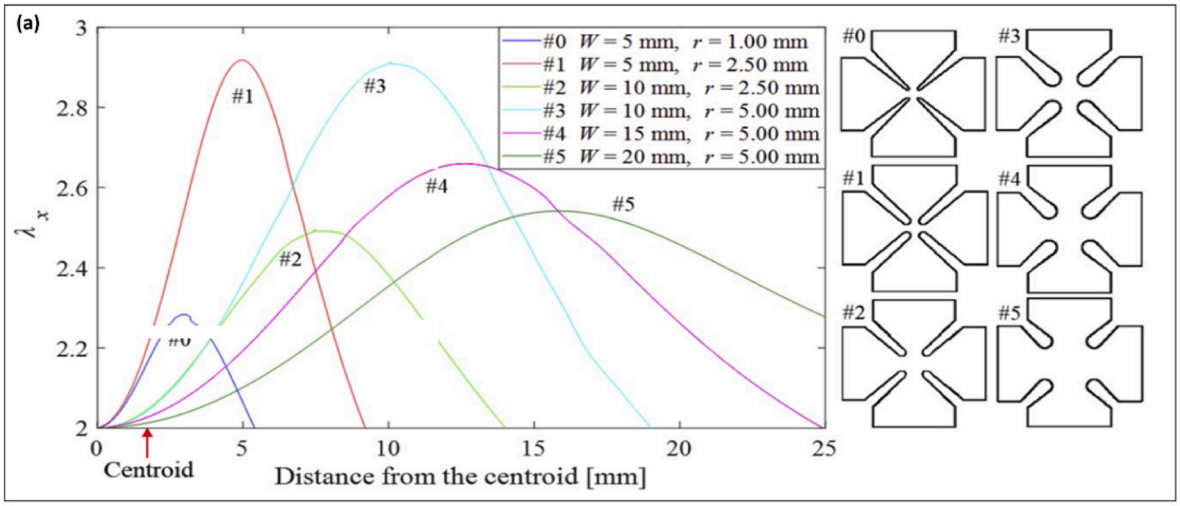


**(b)** FEA result for the specimen shape with $\lambda_x = 2$. Iteration #4, with the lowest $\lambda_{max}$ and highest $\eta$ is selected.

| Iteration | Parameter updated | W (mm) | r (mm) | d (mm) | $\lambda_{Max}$ | Location of $\lambda_{Max}$ | $\eta$ |
|---|---|---|---|---|---|---|---|
| 0 | – | 5 | 1 | 14.8 | 6.2 | Fillet | 0.87 |
| 1 | r | 5 | 2.5 | 22.0 | 4.1 | Arm | 0.69 |
| 2 | W | 10 | 2.5 | 27.2 | 4.5 | Fillet | 0.80 |
| 3 | r | 10 | 5 | 35.2 | 4.1 | Arm | 0.69 |
| 4 (selected in this study) | W | 15 | 5 | 38.0 | 4.1 | Fillet | 0.75 |
| 5 | W | 20 | 5 | 39.0 | 4.7 | Fillet | 0.78 |

**Fig. 5.** Biaxial tension test of a 3D-printed silicone rubber: (a) stretch distribution alongside of the arm from the centroid to the clamped edge and shape change of the specimen in five iterations, (b) FEA results of geometries in 5 iterations [75].

e., W = 15 and r = 5 mm are the best values to reach a proper biaxial state in the middle. It should be noted that a stretch ratio of 2 i.e., elongation of 100% was taken into account in the centroid (Fig. 5b). Specimens 0, 2 and 5 were not selected due to sample failure i.e., the stretches were higher than the ultimate tensile strength (UTS) of the materials. Geometries 3 and 4 manifested acceptable stretch distribution, however the latter showed higher DOE, therefore, it was selected for the biaxial study as optimum sample.

A Digital Image Correlation (DIC) technique was used to measure the Green-Lagrangian strains by mean of the NCORR™ software using equations (6)–(8):

$$\varepsilon_{xx}^{L} = \frac{1}{2}\left(2\frac{\partial u}{\partial x} + \left(\frac{\partial u}{\partial x}\right)^2 + \left(\frac{\partial v}{\partial x}\right)^2\right) \tag{6}$$

$$\varepsilon_{yy}^{L} = \frac{1}{2}\left(2\frac{\partial v}{\partial y} + \left(\frac{\partial u}{\partial y}\right)^2 + \left(\frac{\partial u}{\partial y}\right)^2\right) \tag{7}$$

$$\varepsilon_{xy}^{L} = \frac{1}{2}\left(\frac{\partial u}{\partial x} + \frac{\partial v}{\partial y} + \frac{\partial u \partial u}{\partial x \partial y} + \frac{\partial v \partial v}{\partial x \partial y}\right) \tag{8}$$

where $\varepsilon_{xx}^{L}$ and $\varepsilon_{yy}^{L}$ are the Green-Lagrangian strains in x and y directions, respectively and $\varepsilon_{xy}^{L}$ is the Green-Lagrangian shear strain. Finally, the stretch ratio can be obtained using equations (9) and (10):

$$\lambda_x = \sqrt{\left(2\varepsilon_{xx}^{L} + 1\right)} \tag{9}$$

$$\lambda_y = \sqrt{\left(2\varepsilon_{yy}^{L} + 1\right)} \tag{10}$$

To compare the results with FEM simulation, true strain was calculated using equation (11):

$$\varepsilon_{xx}{}^{T} = \ln \lambda_x \tag{11}$$

The nominal strain, which is the displacement of the grips, d, over the initial length, $L_i$, can be also found using equation (12):

$$\varepsilon_{xx}{}^{N} = 2 \times \frac{d}{L_i} \tag{12}$$

Finally, the apparent true stresses, denoted as $\sigma_{xx}^{Ta}$ and $\sigma_{yy}^{Ta}$, and the approximated true stresses at the centroid denoted as $\sigma_{xx}^{Tc}$ and $\sigma_{xx}^{Tc}$ were obtained using equation (13) and (14), respectively:

$$\sigma_{xx}^{Ta} = \frac{\lambda_x^c F_x}{T_s W} \quad and \ \sigma_{yy}^{Ta} = \frac{\lambda_y^c F_y}{T_s W} \tag{13}$$

$$\sigma_{xx}^{Tc} = S\sigma_{xx}^{Ta} \ and \ \sigma_{yy}^{Tc} = S\sigma_{yy}^{Ta}, \tag{14}$$

in which $F_x$ and $F_y$ are forces in x and y directions, respectively, $T_s$ the thickness, W the width, $\lambda_x^c$ and $\lambda_y^c$ are stretch ratios at the center in x and y directions, respectively, and S is the correction factor obtained by FEM calculation.

Fig. 6a–b shows the strain distribution, $\varepsilon_{xx}^{L}$ and $\varepsilon_{xy}^{L}$ respectively, within the gauge zone at different displacements in the range of d = 0 to d = 38 mm for a 6 mm thick specimen. It is worth noting that the square shape of the gauge region gradually transforms to a circular shape upon stretching the sample resulting from a non-uniform strain distribution in the middle of the cruciform sample. In addition, the circular subset at the centroid ($A_\varepsilon$) manifests more uniform strain distribution with respect to the square gauge zone i.e. a strain variation (the difference between maximum and minimum strains) of 18 % and 102 % for the central subset and the square gauge zone, respectively, are obtained (Fig. 6a and c). This indicates that the former possesses a better equi-biaxial strain state with respect to the latter. Besides, the shear strain, $\varepsilon_{xy}^{L}$, demonstrates almost zero value in the center of the circular subset as shown in Fig. 6b leading to a proper biaxiality. The stretch ratio at the centroid, $\lambda_x^c$ from equation (9), the true strain, $\varepsilon_{xx}{}^{T}$ from equation (11), and the Green-Lagrangian strain at the centroid, $\varepsilon_{xx}^{L}$ from equation (6), with respect to the nominal strain, $\varepsilon_{xx}{}^{N}$ from equation (12), were plotted in Fig. 6d indicating a stretch ratio of 2 can be achieved in the middle of

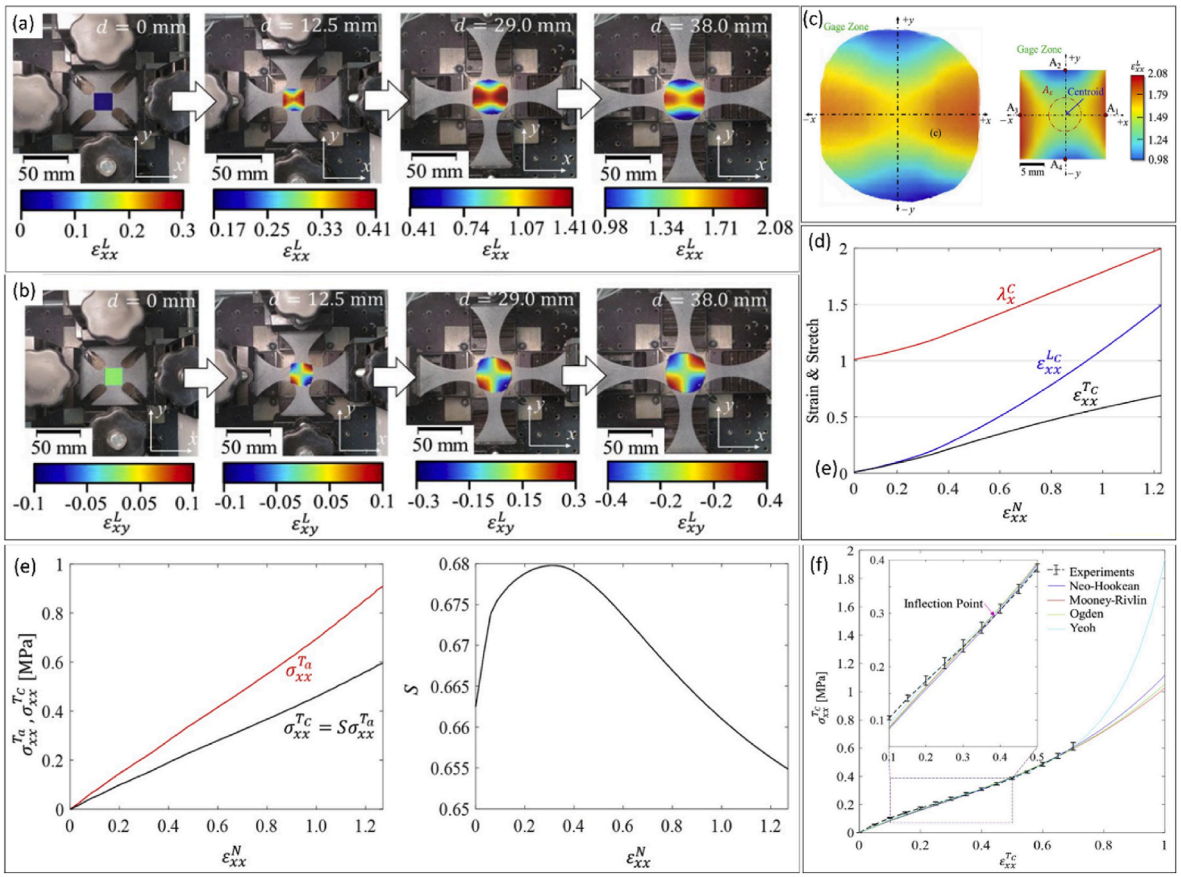


**Fig. 6.** Stress and strain measurement of 3D-printed silicone elastomer: (a–b) Green-Lagrangian strain distributions, $\varepsilon^L_{xx}$ *and* $\varepsilon^L_{xy}$ *respectively, within the gauge zone at different clamp displacements, (c) strain,* $\varepsilon^L_{xx}$*, in the gauge zone in deformed and undeformed states, (d) comparison of stretch ratio, true and Green-Lagrangian strains with respect to nominal strain, (e) apparent true and approximated true stresses versus nominal strain, (f) stress-strain curve from experimental results compared with hyperelastic models* [75]. (For interpretation of the references to colour in this figure legend, the reader is referred to the Web version of this article.)

cruciform sample when a nominal strain of 1.2 (d = 38 mm) is applied. Likewise, the true and the Green-Lagrangian strains diverge at the high nominal strain. The apparent and approximated true stresses versus nominal strains are shown in Fig. 6e. Finally, the stress - strain curve of the biaxial test was compared with the four hyperelastic models as shown in Fig. 6f in which the Yeoh model shows the best fitting followed by Mooney-Rivlin and Ogden models.

Shape optimization of a cruciform specimen made of silicone rubbers reinforced with micro and nano-sized iron particles subjected to a biaxial tension test were studied by Pineda et al. [76]. A combination of Design of Experiment (DOE) and FEM analysis were used to identify optimum geometry as shown in Fig. 7a. Three different parameters were defined to optimize the geometry using the Hammersley optimization algorithm to minimize strain differences between point A and O, as illustrated in Fig. 7a. This was performed to reach a homogenous strain field in the middle. Fig. 7b exhibits optimization outcomes of the three investigated geometries indicating geometry number 2 can achieve higher strain ($\varepsilon_{max}$) and minimum strain difference ($\Delta\varepsilon$), thus, it was selected as the optimum geometry in their study. It can be seen that the modified shape manifests larger and more homogeneous strain distribution compared to the original shape (Fig. 7c).

In another study, Avanzini et al. [80] examined biaxial properties of natural rubbers using different geometries i.e., square-hooks, simple cruciform, cruciform-fillet, cruciform-tapered, cruciform-slits, and uniaxial-rectangle as shown in Fig. 8a. The unstretched and stretched conditions of all specimens are shown in Fig. 8b in which they were stretched until failure of either the specimen or slipping from the grips. All cruciform samples slipped from the grips during biaxial tests whereas the cruciform-slit and square-hook specimens failed from the centre. A cruciform sample with fillet does not show significant difference with respect to the one without fillet, thus, demonstrating no significant effect of stress concentration of the sharp corner in the cruciform sample without fillet. The tapered cruciform specimen shows larger deformation along with cruciform-slit and square-hooks as shown in Fig. 8c. Likewise, the cruciform-slit and square-hooks samples manifest a more uniform deformation in the central region, considering that the shape of the initial central rectangle tends to be maintained which can be attributed to the less constraint on the lateral expansion imposed by weaken arms i.e., with slit and hooks as shown in Fig. 8b. Considering the higher stretch of cruciform-slit and square-hooks samples (Fig. 8c), one can conclude that they can reach a better biaxiality degree. Finally, a FEM analysis was performed taking a Mooney-Rivlin type model by means of inverse method (Fig. 8d) which shows quite good fit with the experimental results demonstrated in Fig. 8c.

Fig. 9a shows the stress distributions at maximum stretch from the same study. Regardless of the cruciform geometry, presence of homogenous stress and stress concentrations in the region far from the edges and in vicinity of the edges, respectively, are notable. Strain distributions are shown in Fig. 9b indicating negligible differences between cruciform samples with and without fillet. Although cruciform-tapered manifested large strain, some inhomogeneity can be seen resulting in less biaxiality in the central region. Finally, the square-hooks sample demonstrates high strain which are evenly distributed. Fig. 9c indicates a very small region of proper biaxiality (homogenous stress) for the cruciform-tapered sample with respect to other samples showing relatively high variations on the edges but better biaxiality in the middle. As

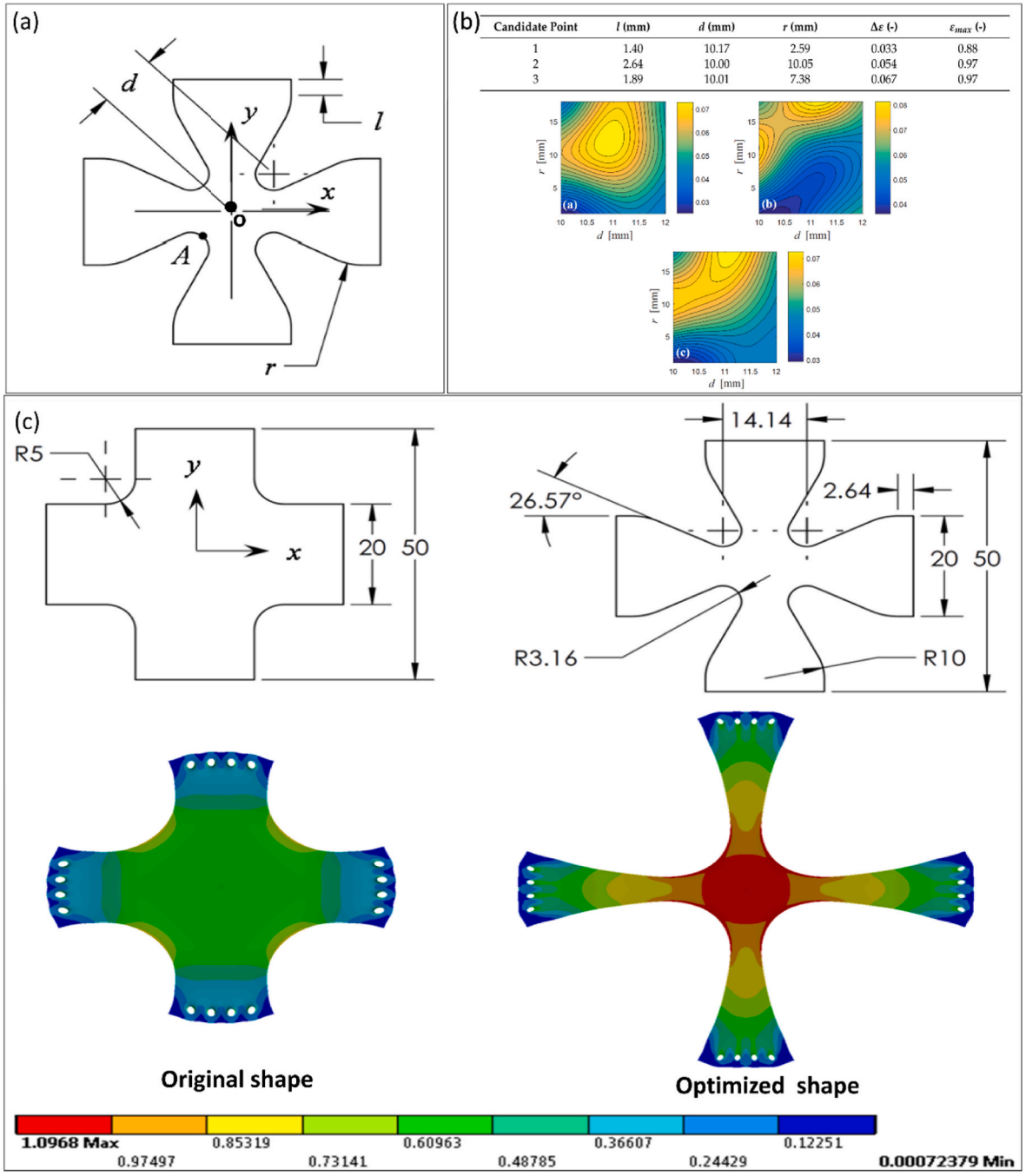


**Fig. 7.** Equi-biaxial tension test of reinforced magnetorheological elastomers with micro- and nanoparticles: (a) input variables for the Hammersley optimization algorithm, (b) optimization results of three different geometries (c) comparison of equivalent strain distribution in two different cruciform geometries [76].

mentioned earlier, a larger area of uniform deformation in the middle with respect to the central area results in a better biaxiality.

A uniform-biaxiality index denoted as $R_{biax}$ is defined in equation (15) which is shown in Fig. 9d–e. The contour map shown in Fig. 9d indicates that the area with the absolute differences less than 0.05 in $E_{xx}$ and $E_{yy}$ are coloured i.e., blue colour is not biaxial region. It can be concluded that a bigger region of the proper biaxiality is achieved for the square-hooks and cruciform-slit samples whereas the cruciform-tapered manifested the lowest biaxiality index. Finally, a stress correction factor was defined (equation (16)) which was used as a criteria to show the efficiency of load transferring from the grip area to the middle (Fig. 9f). It was revealed that the cruciform-slit sample possesses the most uniform stress distribution as the correction factor is nearly one.

$$R_{biax} = \frac{\left(\frac{E_{xx}+E_{yy}}{2}\right)}{(E_{max})_{0,0}} \tag{15}$$

$$Correction\ factor = \frac{1st\ Piola\ stress}{Nominal\ stress} \tag{16}$$

where $E_{xx}$ and $E_{yy}$ strains in x and y directions, respectively, and $E_{max0,0}$ is maximum strain in the centre. It should be noted that the Piola stress was calculated at the central region using FEM while nominal stress was obtained based on the initial dimensions.

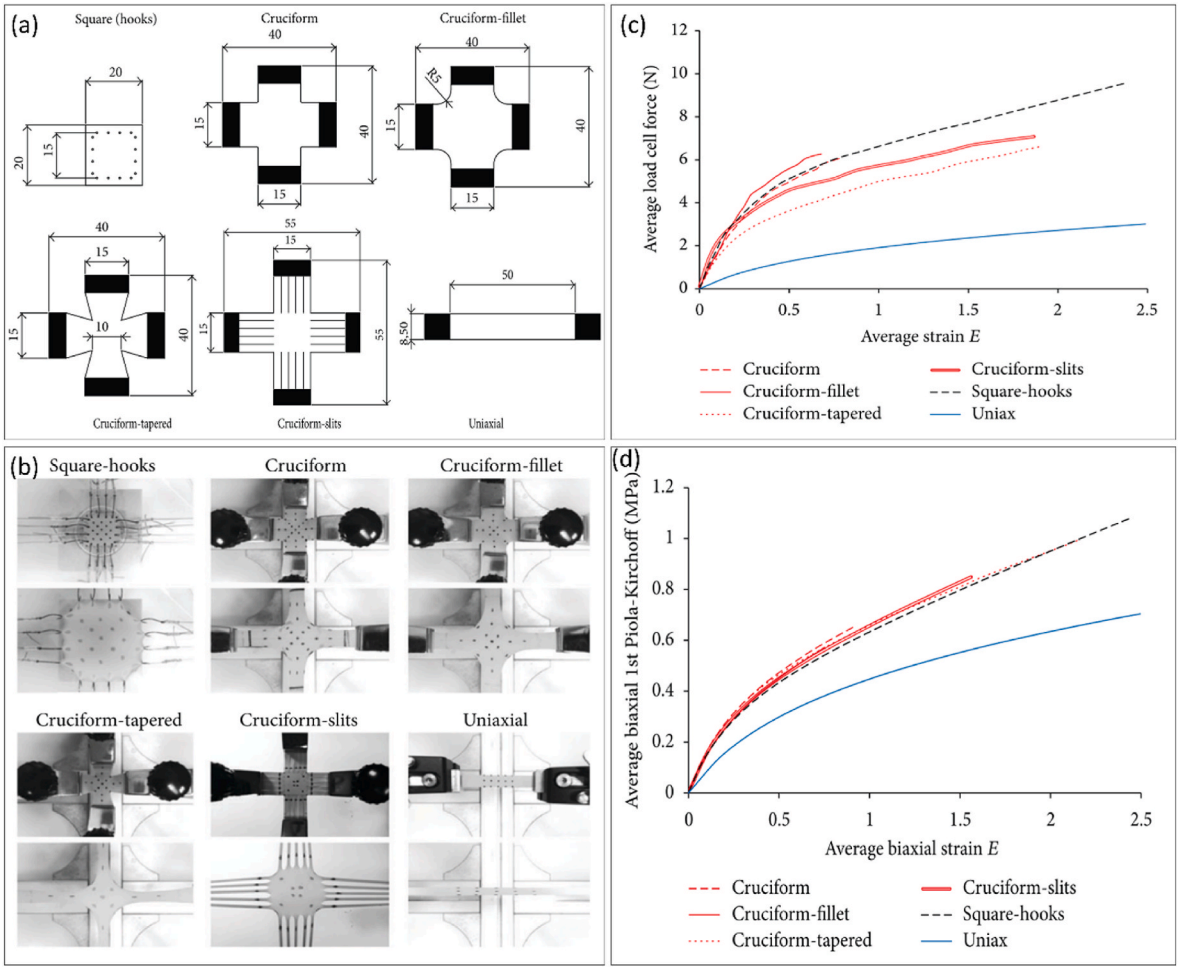


**Fig. 8.** Experimental and numerical biaxial characterizations of natural rubber: (a) different gripping systems and sample geometries, (b) unstretched and stretched samples, (c) force-strain in real experiment, (d) stress-strain curves using FEM calculation [80].

## 4. Biaxial test methodologies and results

This section is divided into two main subsections including elastomers and hydrogels in which their viscoelastic and fracture properties are separately reviewed in detail. It is worth noting that since there is no specific standard for biaxial characterization, different test setups were employed in the literature. Therefore, in this section, the test procedure for biaxial test characterization of soft polymers will be briefly reviewed including loading conditions i.e., pure shear (PS), equi-biaxial (EB) and unequal-biaxial (UB), strain rate, strain amplitude, clamping systems, and the final outcomes. Table 1 summarizes some of the notable works conducted in biaxial conditions using square and cruciform samples. From Table 1, it can be seen that different shapes, loading conditions and various test setups were used. In addition, some studies used reinforcement in the edges using separate parts or by thickening the edges via moulding [68,74,78,83,94]. In the following sections, some of the studies listed in Table 1 are briefly reviewed.

### 4.1. Biaxial tests on soft polymers

#### 4.1.1. Experiments for hyper-viscoelastic characterizations

Biaxial properties of a 3D printed hyperelastic photopolymer known as TangoBlackPlus (70% elongation at break) was investigated by Moris et al. [68]. The test was performed with a strain rate of 0.05 mm/s where: (i) the specimen was pre-stretched in y-direction resulting in a uniaxial deformation in this direction, (ii) keeping the y-displacement fixed, the displacement in the x-direction was increased stepwise until the sample failure (Fig. 10a). A relaxation time of 90 s was considered between each stepwise increase. A cut of 3.5 mm was created (Fig. 2a) to isolate the griping area from the centre resulting in a more uniform and larger strain in the middle of the specimen. On the other hand, this is disputable because creating a cut on the corner of cruciform sample imposed further stress around the cut, thus, acts as a pre-crack, which results in earlier failure collinear to the cut rather than achieving proper biaxiality.

Pre-stretching in y-direction resulted in an induced force increase in both directions followed by a stepwise force increase in both directions upon a stepwise displacement increase in the x-direction (Fig. 10a–b). Fig. 10c manifests the uniform strain distribution within the center of a cruciform specimen. In addition the preliminary strain in the x-direction exhibits a negative value after pre-stretching in the y-direction (Fig. 10d). The stepwise increase of displacement resulted in strain increase in the x-direction whereas a slight increase in the y-direction took place. According to their results, the coefficients of the Moony- Rivlin model can be thoroughly obtained from biaxial test due to high amount of deformation states.

One of the typical phenomena in filled elastomers is Mullins effect in which most of the previous studies were investigated in uniaxial mode [126]. In an effort made by Mai et al. [69], this feature was probed in biaxial and planar modes for a Styrene Butadiene Rubber (SBR) reinforced with silica particles as hwon in Fig. 11a.A crosshead speed of 0.25 mm/s was used for the biaxial test. A relaxation time of 30 min was considered between unloading and reloading in which an equilibrium strain state was achieved. The stress-strain curves of various filled SBR

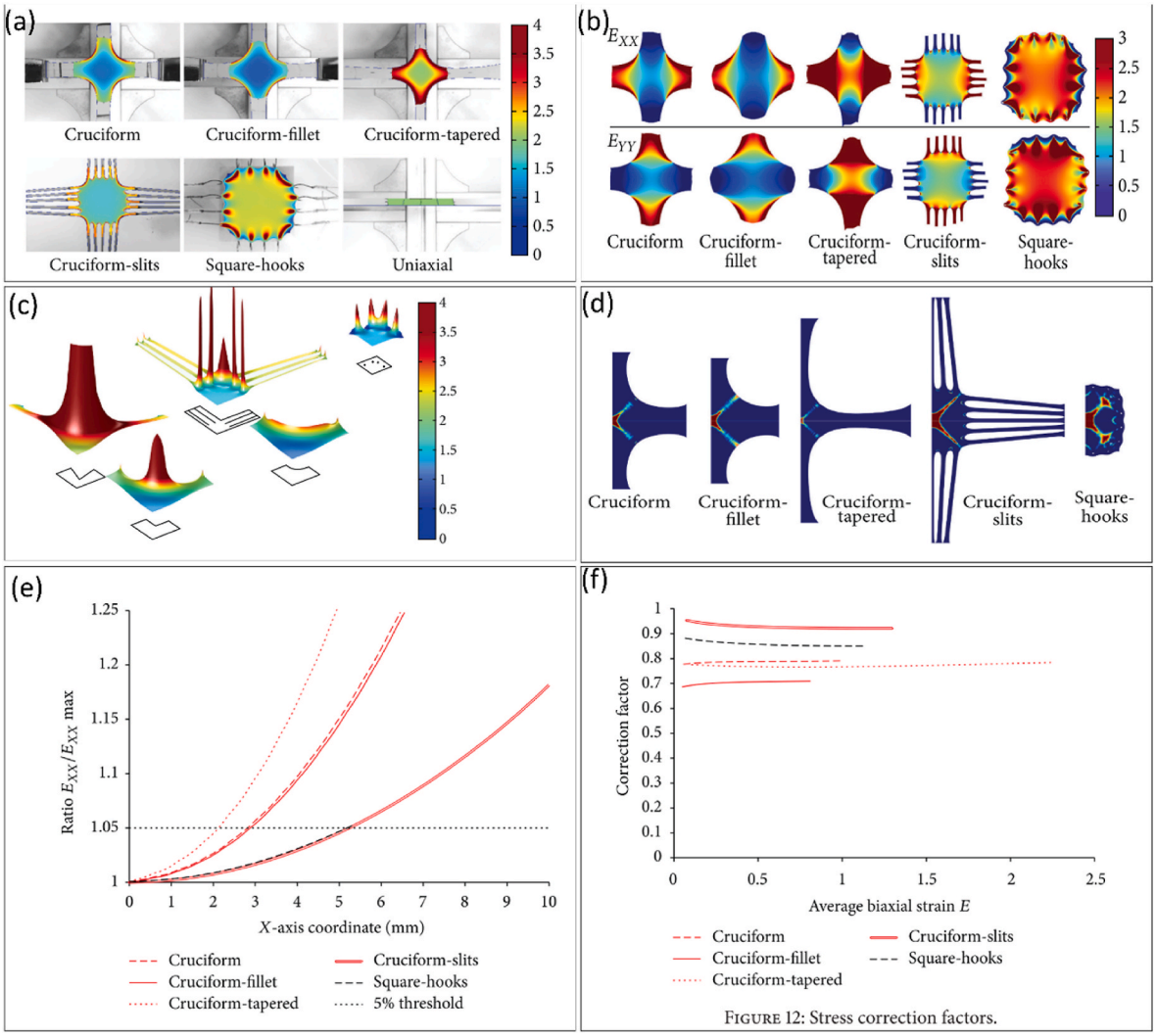


**Fig. 9.** Strain and stress distributions along with biaxiality index and stress correction factors: (a) Von Mises stress distribution laid over on real stretched samples, (b) Green-Lagrange strains distribution, (c) Von Mises stress distribution for initial shape of the specimen,(d) biaxiality index, (e) variation of biaxiality index along x-direction in the middle, (f) stress correction factor [80]. (For interpretation of the references to colour in this figure legend, the reader is referred to the Web version of this article.)

are shown in Fig. 11c–e where a pronounced stress increase can be distinguished for equibiaxial and planar samples with respect to the uniaxial test. The failure of the specimen is denoted by cross symbol in Fig. 11b, though they did not indicate whether the sample are ruptured from the gauge region (the middle region for EB and PE test) or it was slipped from the grip. As mentioned earlier, one of the main challenges in performing reliable biaxial test is to make sure that the sample fail from the gauge zone i.e. the middle area for either cruciform or square samples. Therefore, the failure location of specimen should be reported in any biaxial test so that the reliability of test can be verified. In addition, all samples were subjected to a cyclic loading-unloading conditions with stepwise increase of stretch (λ) from 1.1 to 3 for the investigation of Mullins effects as shown in Fig. 11c–e in which the presence of the Mullins effect is quite notable for all samples. It is worth to note that residual strain and dissipated energy are highest (at the same elongation λ) in EB, followed by PS and uniaxial (U) conditions.

Heterogeneity and anisotropy are another pronounced characteristics of soft polymers, especially for filled elastomers, 3D-prited soft polymers and soft tissues [127–130] which need to be further investigated thought biaxial tests. In this context, Johlitz et al. [70] studied anisotropic behaviour of silicone elastomers, prepared by open moulding, using biaxial test. Fig. 2c shows the geometry of the cruciform samples with the thickness of 1.65 mm. Two experimental setups were used i.e., set-1 was pre-stretched in x-direction from 0 to 30 mm with the step of 6 mm while the other axis was subjected to a 3 mm stepwise continuous loading at each pre-stretch. The set-2 experiment was reverse (Fig. 12a). It can be concluded that the developed sample was isotropic since the force in both sets of experiments are the same. Fig. 12b–c show the change in force and stretch with respect to time, respectively, in both directions when subjected to 18 mm pre-stretch (direction 1 is pre-stretched while a continuous loading was applied in the direction 2). Upon pre-stretching, the force and stretch in direction 1 (left curves in Fig. 12b–c) abruptly increase resulting in a slight increase in force and stretch in the direction 2 i.e., $\lambda < 1$ (right curve in Fig. 12b–c). Stepwise increase of the load in direction 2 leads to a significant increment of the load and stretch in this direction whereas a slight increase in force and stretch can be seen in the pre-stretched direction. The importance of running biaxial test for soft materials to identify materials heterogeneity can be well recognized indicating the necessity of having proper guidelines for biaxial characterization.

In line with studying anisotropic behaviour of elastomers, Kodaira et al. [82] studied anisotropic characteristics of a polyvinylidene difluoride (PVDF) flat membrane. Due to anisotropy arisen from the injection direction in moulded samples, the injection direction was

**Table 1**
A summary of biaxial tests performed on various soft polymers.

| Material | Shape[b] | Dimension (mm) | Test type[a] | Strain rate or speed*** | Grip region | Ref |
|---|---|---|---|---|---|---|
| **Elastomers** | | | | | | |
| **Silicone** | Cr, Sq | … | EB | 1.3 mm/s | … | [25] |
| **Photopolymer (TangoBlackPlus)** | CR | 67 × 67 | UB | 0.05 mm/s | Reinforced | [68] |
| **SBR** | Sq | 70 × 70 × 2 | EB, PS | 0.25 mm/s | … | [69] |
| **ELASTOSIL® RT 265** | Cr | 75 × 75 × 1.65 | UB | … | …. | [70] |
| **NR** | Cr | 165 × 165 × 3 | UB | 0.5 mm/s | Reinforced | [71] |
| **NR** | Cr | 39.5 × 49.5 × 2 | UB | 2.5 mm/s | …. | [72] |
| **ELASTOSIL ® RT 625** | Cr | 67 × 67 | EB | … | …. | [73] |
| **Polypropylene/polyethylene** | Cr | 140 × 140 × 0.6 | EB | 0.1 mm/s | Reinforced | [74] |
| **Silicone** | Cr | 87 × 87 × 2 | EB | 0.03 mm/s | … | [75] |
| **Reinforced magnetorheological elastomers (MRE)** | Cr | 50 × 50 | EB | …. | …. | [76] |
| **Poly Ethylene Terephthalate** | Cr | 110 × 110 × 4 | EB | 100 mm/s | … | [77] |
| **SBR** | Sq | 77 × 77 × 1.85 | EB,PS | 1 Hz | Reinforced | [78] |
| **Rubber** | Sq | 20 × 20 × 0.5 | EB | 0.1 mm/s | … | [80] |
| | Cr | 55 × 55 × 0.5 | | | | |
| **Latex, Oppo band, Ecoflex** | Sq | 7 × 7 × 0.25 | UB | 0.28, 0.06,0.04 | … | [81] |
| **NBR** | Sq | 60 × 60x | EB | 1.6 | | [82] |
| **NRE211 film** | Cr | 38 × 38 × 0.027 | EB,UB,PS | 0.014 | Reinforced | [83] |
| **Silicone** | Cr | 63.5 × 63.5 × 0.5 | EB | 0.63 | … | [86] |
| **MREs** | Sq | 50 × 50 × 2 | EB | 0.16 mm/s | … | [95] |
| **Isoprene rubber (IR)** | Sq | 115 × 115 × 1 | EB | … | … | [96] |
| **Poly(dimethylsiloxane) (PDMS)** | Sq | 40 × 40 × 0.5 | EB | … | Thickness optimized | [97] |
| **Thermotropic liquid-crystalline polymer (TLCP)** | Sq | 12.5 × 12.5 × 1 | EB | 0.01 1/sec | … | [98] |
| **Cholesteric elastomers** | Sq | 10 × 10 × 0.02 | EB | … | … | [99] |
| **VHB polyacrylic elastomer** | Sq | 10 × 10 × 0.02 | EB | 0.025, 0.05, 0.075, 0.1, 0.2, 0.3 (1/sec) | … | [100] |
| **Hydroxy- terminated polybutadiene (HTPB)** | Cr | 50 × 45 × 5 | EB | … | .. | [101] |
| **Propellants** | Cr | 50 × 45 × 5 | EB | … | .. | [102] |
| **NR** | | 75 × 75 × 0.5 | EB | 0–0.7 mm/s | .. | [103] |
| **VHB and Ecoflex** | Sq | 70 × 70 × 1 | EB | 0.3 1/sec | … | [104] |
| **Latex** | Sq | 7×7×(th: 0.25, 0.5,1) | EB,UB | 0.43%/s, 4.3%/s, 10%/s | … | [105] |
| **CNT/polyolefin elastomer** | Cr | 80x80x1 | EB | 10 mm/s | . | [106] |
| **SBR-1500** | Cr | 125x125x2 | EB | 25%/min | … | [107] |
| **Elastomeric scaffolds** | Sq | 12x12 | EB | 10 mm/min | . | [108] |
| **NR** | Cr | 50x50x2 | EB | 6 mm/min | … | [109] |
| **Silicone elastomers** | Sq | 50x50x1 | EB | … | .. | [110] |
| **NR** | Cr | 63.5x63.5x0.3 | EB | …. | … | [111] |
| **SBR** | Sq | 70x70x0.8 | PS,EB | 0.2 mm/s | … | [112] |
| **NR** | Sq | 60x60x2 | EB | 0.001 1/sec | .. | [113] |
| **NR** | Sq | 70x70x1.2 | EB | … | … | [114] |
| **NR** | Cr | 190x190x1 | EB | … | … | [115] |
| **NR** | square | 131x131x3 | EB | 60 mm/s | | [116] |
| **Ecoflex** | square | 131x131x3 | EB | 60 mm/s | | [117] |
| **PDMS** | Cr | 40.75x5x0.6 | EB | … | … | [118] |
| **Hydrogels** | | | | | | |
| **Hydrogels** | Sq | 65 × 65 × 1.5 | UB,EB,PS | 1 mm/s | … | [79] |
| **Hydrogels** | Sq | 65 × 65 × 2 | EB,PS | 1 mm/s | … | [84] |
| **Hydrogels** | Sq | 65 × 65 × 2 | EB,UB,PS | 1 mm/s | … | [85] |
| **PTHF and PDMS gels** | Sq | 65x65x1 | EB | 0.002, 0.004 1/sec | …. | [119] |
| **Bacterial cellulose hydrogel** | Cr | 40x40x3 | EB | 0.067 1/sec | .. | [120] |
| **Double network hydrogels** | Sq | 65x65x1.5 | EB,UB | 0.1, 0.2,0.5,0.8,1,1.6 mm/s | .. | [121] |
| **Poly(vinyl alcohol) (PVA) gel** | Sq | 40x40 | EB | … | … | [122] |
| **(PAAm) Hydrogels** | Sq | 65×65×2 | EB | 1 mm/s | … | [123] |
| **Tetra-PEG gel** | Sq | 50 × 50 × 2 | EB | 1 mm/s | .. | [124] |
| **Polyrotaxane-based slide-ring (SR) gels** | Sq | 65x65x1.5 | UB | 1 mm/s | | [125] |

[a] EB: Equi-Biaxial; PS: Pure Shear; UB: Unequi-Biaxial.
[b] Cr: Cruciform; Sq: Square.

considered at 90° whereas vertical direction was defined at 0°. An evaluation area of 20 × 20 $mm^2$ was considered to guarantee a homogenous strain distribution as shown in Fig. 13a. A strain rate of 1.66 × $10^{-2}$ 1/sec was used for all tests. The uniaxial and biaxial characterizations of PVDF manifest anisotropic behaviour as the stress-strain curves in two directions are not matched (Fig. 13b–c). In addition, both uniaxial and biaxial tests indicate the yield strength in 0° direction is greater than 90° direction. It is worth noting that a material subjected to biaxial stress can be considered as yielded if the material yields in any direction. Therefore, they have performed a biaxial test with strain ratio of 2:1, i.e., the strain ratio in 0° is twice as that of 90° (Fig. 13d–e). The yield strength was obtained using proof stress (0.2 % strain) in both directions as shown in Fig. 13d. The stress-time curve (Fig. 13e) was used to obtain the yielding time in both directions. Since the strain rate in 0° direction was twice than 90°, the yield time was smaller. It was concluded that the yielding strength in 90° should be obtained at the same time of yielding in 0°.

In order to understand the dissipative behaviour of natural rubbers, Dedova et al. [131] investigated energy dissipation of oil-extended solution styrene butadiene rubber (SSBR) filled with 50 phr carbon-black particles subjected to biaxial tension. In this case, specimens were pre-stretched equi-biaxially up to 120 % strain at 1 Hz for 30 cycles to reduce Mullins effect. Then, the samples were loaded quasi-statically (0.1 mm/s) up to the same strain imposed during cycling loading. The dynamic loading and unloading test was performed using a triangular waveform in four different settings including PS, EB, Asymmetrical

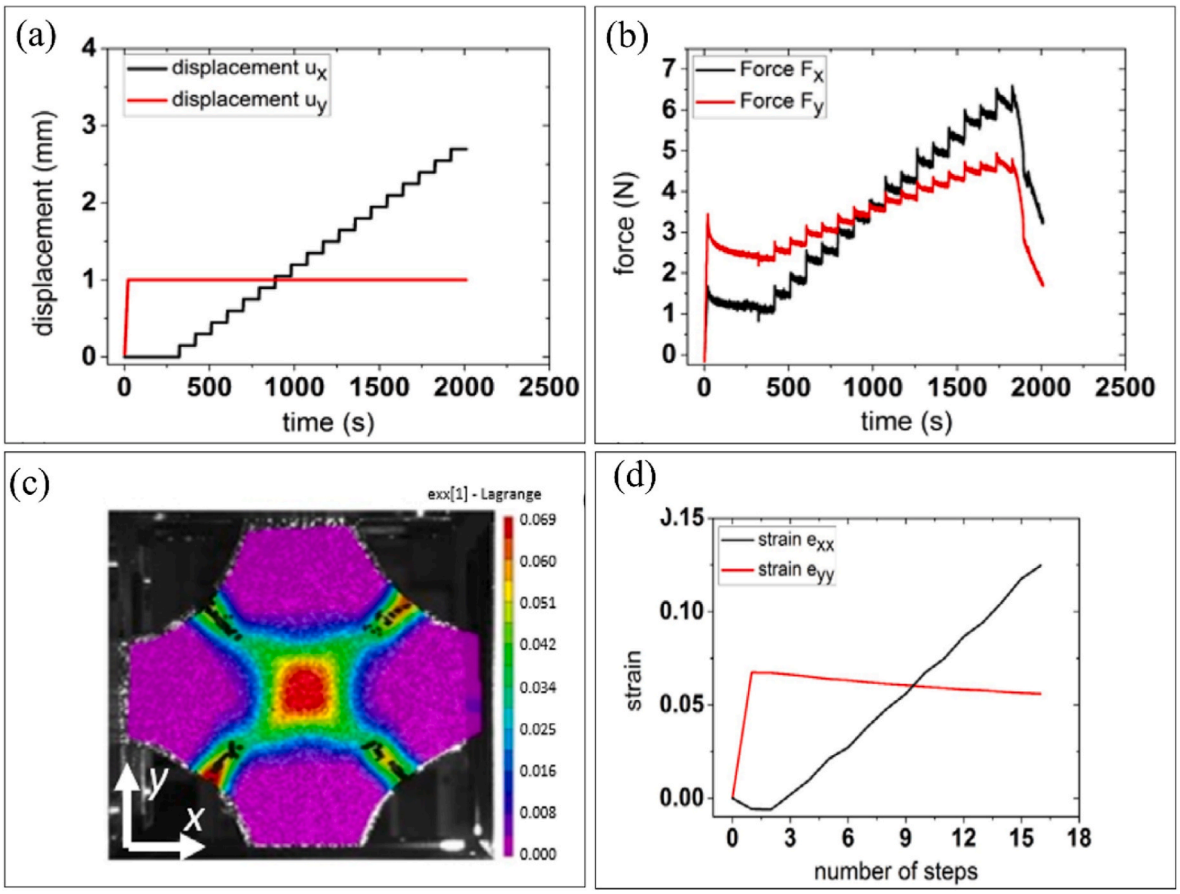


**Fig. 10.** Biaxial test results (a) displacement versus time, (b) force versus time, (c) strain distribution, (d) strain versus time [68].

Biaxial (AB) and Uniaxial (U). For the AB, the strain in x-direction was twice than that in y-direction. The stress-strain curve of the last loading-unloading cycle i.e., cycle number of 300, at different conditions are shown in Fig. 14a. Regardless of the loading condition and strain amplitude, all samples show hysteresis loss; in addition to increasing softening effect when the applied strain amplitude increases. The dissipated energy is the same for all deformation states if an equivalent von Mises strain is considered (Fig. 14b). Further, they have also investigated biaxial characteristics of SBR filled with 20 phr carbon-black using a square specimen with beading bulge at the edges [132]. Two different clamping systems were designed for samples with uniform and non-uniform thickness in the edge as shown in Fig. 14c. This was done to obtain the optimum design for the sample edges as well as clamping systems to avoid stress concentration in the edges and to guarantee larger area of uniform strain distribution in the middle can be achieved. According to their results, sample with thicker edges and associated clamping systems shown in Fig. 14c reaches much better biaxially degrees. This finding is substantially important to reach proper biaxial test, for high cyclic fatigue test when reinforcing sample edges and proper gripping are very crucial.

In addition to Mullins behaviour and energy dissipation of elastomers under biaxial mode that mentioned earlier, the rate dependency of the elastomer is also important characteristic that need to be studied. In an effort to understand the rate-dependency behaviour of soft polymers, Meredith et al. [83] investigated biaxial properties of Nafion membrane (a brand name for a *sulfonated tetrafluoroethylene based fluoropolymer-copolymer*) subjected to tension loading. The strain was obtained in the middle of the sample using a DIC device as shown in Fig. 15a. Three different biaxial ratios were considered based on equation (17):

$$B = \frac{\dot{\lambda}_1}{\dot{\lambda}_2} \tag{17}$$

where $\dot{\lambda}_1$ and $\dot{\lambda}_2$ are the stretching rates in directions 1 and 2, respectively. A strain rate of 14 μm/s was used in both directions for B = 1 (equi-biaxial) whereas the strain rate in the direction-1 was half of direction 2 at B = 0.5. The movement in the direction 1 was constrained for B = 0. Fig. 15b shows the top right region of the cruciform specimens prior to and after deformation in which the sample is subjected to different biaxial ratios resulting in a concave curvature. Finally, the true stress-strain curves under static condition (Fig. 15c) for all biaxial ratios indicate elastic-viscoelastic behaviour quite similar to a uniaxial test i.e., an initial elastic region followed by a nonlinear strain hardening region. For equi-biaxial condition (B = 1), the elastic modulus and yield stress are larger than the one in the uniaxial test (Fig. 15c). The stress in direction 1 decreases with respect to direction 2 for B = 0.5 and B = 0 resulting from its lower strain rate. In addition, a reduced yield strength hysteresis pattern can be detected for all cyclic biaxial conditions (Fig. 15d–f).

#### 4.1.2. Experiments on fracture characterizations

Elastomers are typically subjected to alternating loading conditions in which final fatigue failure is attributed to crack initiation and crack propagation [133]. The ability of an elastomer to resist against crack propagation is called fracture toughness, which is one of the most important properties of elastomers. Therefore, some studies evaluated fracture properties of elastomers in biaxial mode which is typical loading scenarios of them. In this context, Marano et al. [71] conducted extensive investigation to understand the mode I fracture toughness of carbon black-filled natural rubbers with different filler concentrations

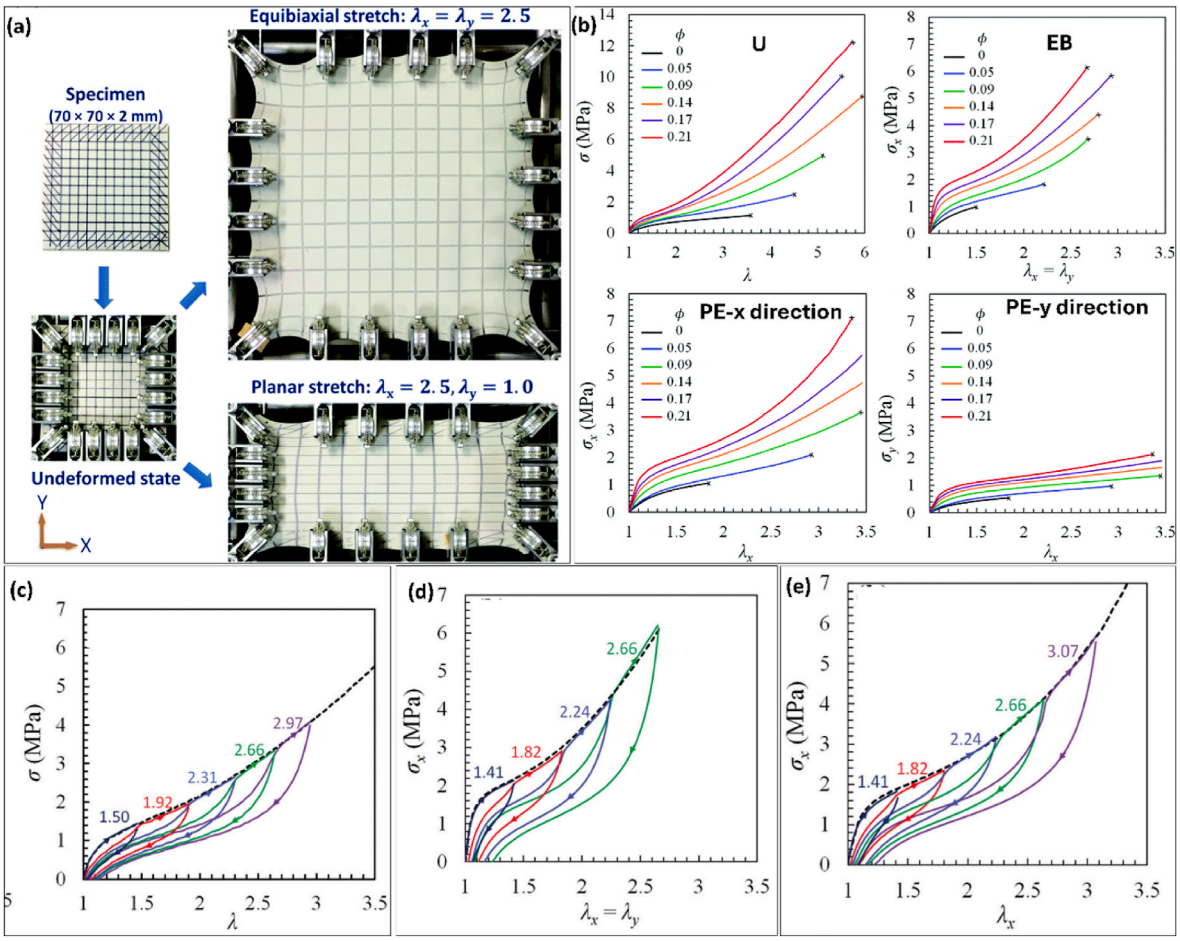


**Fig. 11.** SBR/silica (ø = 0.21) subjected to biaxial cyclic loading: (a) equi-biaxial and planar setups, (b) stress-strain curves to the failure for uniaxial, equibiaxial and planar modes, (c–e) stress-strain curves at uniaxial, equibiaxial and planar modes, respectively, [69].

under biaxial loading using a cruciform specimen (3 mm thickness) as shown in Fig. 16a. For the experimental study, natural rubbers filled with 25, 50, and 75 phr carbon black were prepared in which a 4 mm crack was introduced in the middle of the cruciform sample (Fig. 16a). The biaxial test was performed in two stages including pre-stretching the sample in direction 2 up to $\lambda < 2.5$, followed by loading continuously in the direction 1 until final failure (Fig. 16b). The fracture toughness was obtained using equation (18):

$$K_{IC} = \sigma_c \sqrt{\pi \times a} \tag{18}$$

where $2a = \lambda_2$. $a_0$ is the notch length prior to the final failure (with the onset of crack propagation), $a_0$ is the initial notch length in the direction 2 and $\sigma_c$ is the critical stress in the direction 1 (perpendicular to the notch plane upon the onset of crack propagation). Two different types of crack growth can be distinguished including forward crack (along the notch plane) and two sideways crack perpendicular to the notch plane as shown in Fig. 16c–d, respectively. For the unfilled natural rubber (NR0), regardless of the induced stretch in the direction 2 ($\lambda_2$), the crack growth takes place only in the forward direction and $K_{IC}$ decreases slightly in the response of $\lambda_2$ (filled squares in Fig. 16e). Similarly, filled rubbers manifest forward crack propagation at high stretch in which $K_{IC}$ approaches a constant value irrespective of $\lambda_2$ (filled squares in Fig. 16f–h). However, the fracture toughness obtained from the onset of forward crack at a low stretch shows significant changes as a function of $\lambda_2$ (open squares in Fig. 16f–h) while the $K_{IC}$ related to the onset of sideway crack shows only a slight change (filled circles in Fig. 16f–h). It can be concluded that fracture resistance of elastomers can be thoroughly evaluated in biaxial modes which can be very useful information especially for dielectric elastomers [100,104]. However, lack of standardized procedure for biaxial characterization aiming to investigated viscoelastic, anisotropic, energy dissipation, fracture toughness and fatigue properties of elastomers resulted in various testing parameters as discussed earlier. For instance, a 4 mm pre-crack length was used in Marano et al. [71] for fracture toughness characterization, however a 16 mm pre-crack was induced into an square sample studied by the same authors in another study [116].

### 4.2. Biaxial tests on hydrogels

#### 4.2.1. Experiments for hyper-viscoelastic characterizations

Extremely soft hydrogels have been experimentally characterized using biaxial loading conditions. For instance, Mai et al. [79] investigated characteristics of hydrogels in different loading conditions including uniaxial and biaxial tension tests as shown on Fig. 17a. The crosshead speed in x-direction was double than that of y-direction in the unequal biaxial (UB) sample. In addition, for the unidirectional test (U), a specimen with the dimension of 65 × 6.0 × 1.5 $mm^3$ and the gauge length of 35 mm was prepared while a crosshead speed of 0.70 mm/s was used. As it can be seen from Fig. 17b, the stress in response to equi-biaxial (EB) strains is the highest followed by UB, PE (planar), and U conditions. In addition, Mullins effect can be clearly seen for all time-dependent loadings as shown in Fig. 17c–f. The residual strain increases as a function of applied stretch, though it is negligible at a very low strain. It substantially increases at high strains (Fig. 17g). Moreover, the initial elastic modulus of each deformation state at its corresponding stretch was obtained from the initial slope of the reloading stress-strain

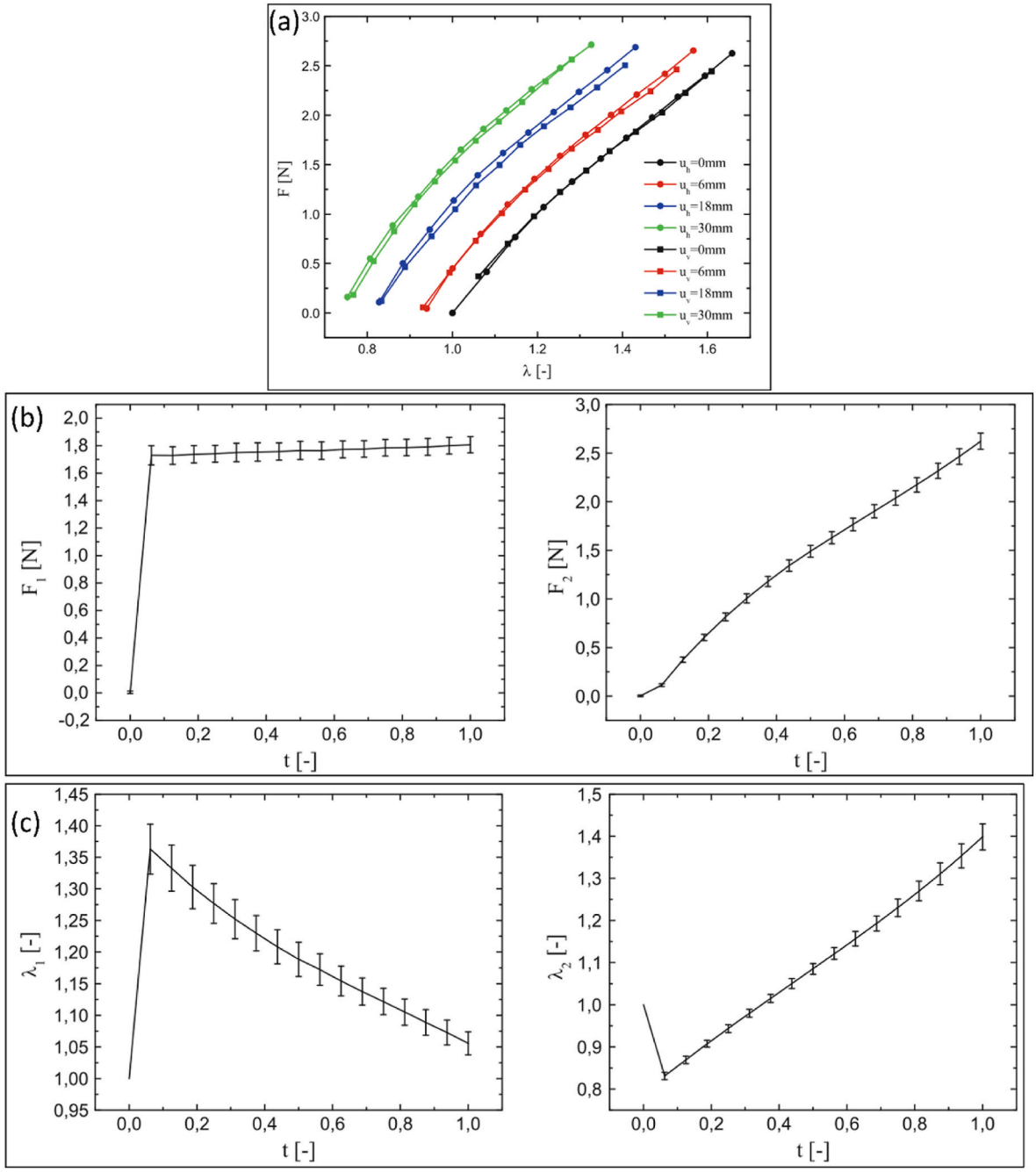


**Fig. 12.** Biaxial tension characterization of silicone rubber: (a) force-stretch in biaxial loading, (b–c) force-time and stretch-time in fixed prestretch of 18 mm respectively [70].

curve at a low strain denoted as $A^i$ whereas $A_0$ is the elastic modulus of the virgin loading. The elastic modulus and its ratio $\frac{A^i}{A_0^i}$ decrease in response to stretching and become insensitive to the state of deformation at large stretches (Fig. 17h–i). Finally, the dissipation energy, input work, and dissipation factor (the ratio of dissipation to input work) denoted as D, W, and Δ, respectively, subjected to a single cycle are shown in Fig. 17j-m. It can be concluded that EB manifests the highest dissipation factor followed by UB, PE, and U and a critical strain known as the threshold value, the dissipation factor increases dramatically. The study reported a critical strain, denoted as $\lambda_x^c$ equals to 1.03, 1.06, 1.08, and 1.12 for EB, UB, PE, and U, respectively.

Biaxial properties of an extremely soft polymer gel known as poly (acrylamide) (PAAm) hydrogel in pure shear and equi-biaxial modes were investigated by Yohsuke et al. [84]. Fig. 18a shows the extremely soft hydrogel as its self-weight induces bending resulting from its very low modulus typically in the range of 102 Pa. Therefore, the biaxial test was conducted in the solvent bath to avoid initial bending by self-weight (Fig. 18b). A crosshead speed of 1 mm/s was used for the uniaxial and biaxial tests. The nominal principal stress versus principal stretch is shown in Fig. 18c whereas a more detailed view at $\lambda < 1.3$ is shown in Fig. 18d. No differences can be seen in the EB test in both directions manifesting a uniform strain was applied in the middle of the sample. In addition, a linear stress-strain region is obtained at small elongation for all deformation states as shown in Fig. 18d, which can be used to find the initial modulus of the sample. The initial modulus obtained by the slope of the curves in that region agrees well with the one obtained by the linear elasticity theory.

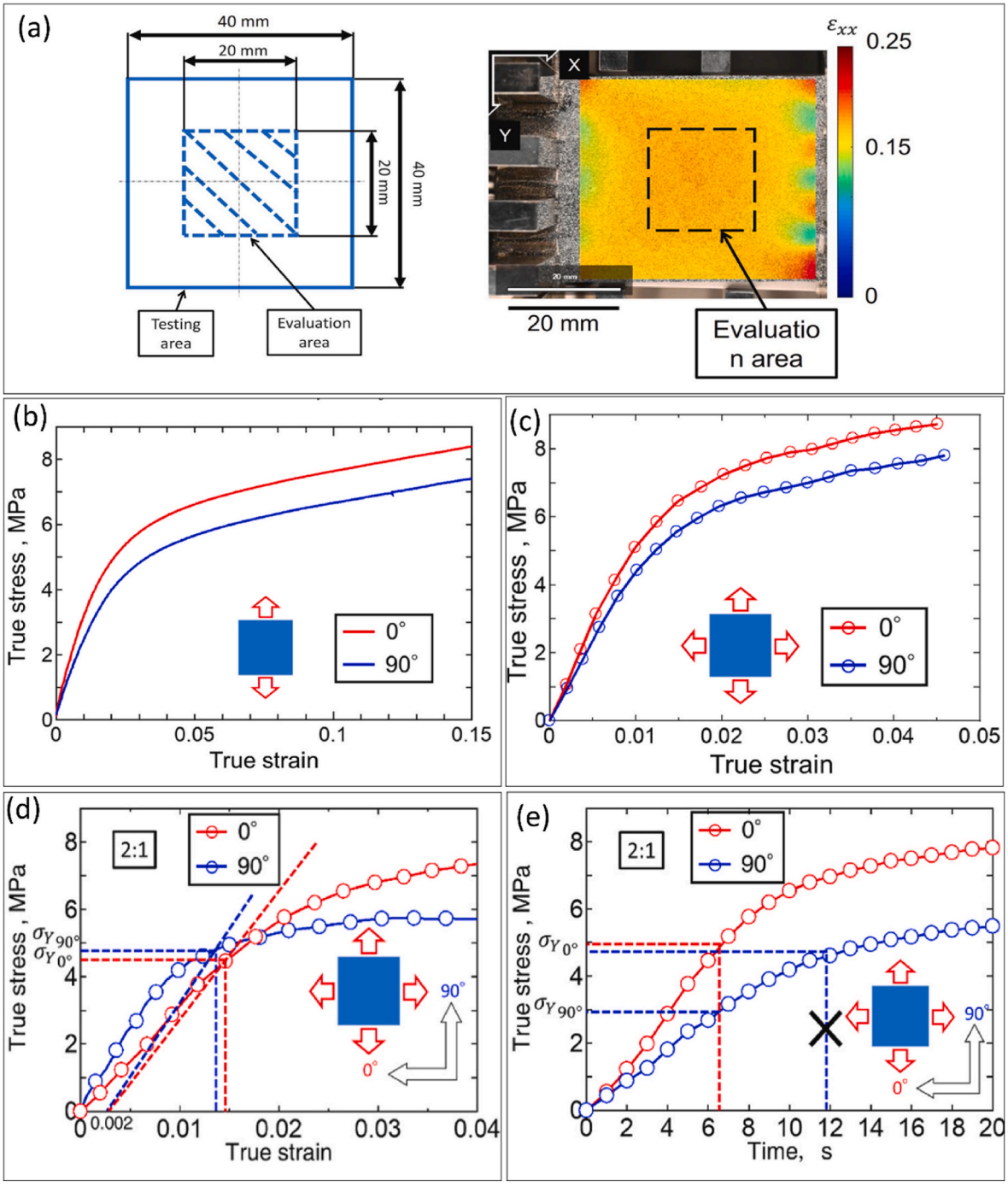


**Fig. 13.** Uniaxial and biaxial characterizations of porous polymer membranes: (a) examination area of the biaxial test, (b–c) true stress-true strain during uniaxial and biaxial tests, respectively for polyvinylidene difluoride (PVDF), (d–e) true stress-strain and true stress-time, respectively, in biaxial test at strain ratio of 2:1 [82].

*4.2.2. Experiments for fracture characterizations*

In addition to traditional rate-dependent viscoelastic experimentations of polymers and hydrogels, Mai et al. [85] conducted an extensive campaign to reveal the fracture behaviour of soft hydrogels. For instance, strain energy release rate and crack tip strain field distribution of PDMA hydrogel subjected to different biaxial loadings including PS, UB and EB were investigated by the same authors [85]. The samples were tested with a crosshead speed of 1 mm/s in both x- and y-directions for EB whereas the crosshead speed of 0.5 and 0.0 mm/s were used in the x-direction for UB and PE specimens. In addition, single edge notched samples with different initial notch lengths ($X_c$) in the range of −10 to +10 mm (with respect to the specimen centre) were also introduced for the measurement of strain energy release rate as shown in Fig. 19a. It is worth noting that $X_c = -5$ mm was selected for the strain field measurement for single edge notched samples subjected to biaxial loading. Biaxial characterization of the sample without a notch was also performed as shown in Fig. 19b. The EB sample possesses higher nominal stress ($\sigma_y$) followed by the UB and PE samples when compared at the same $E_y$ (the cross mark in nominal stress-nominal strain in Fig. 19b point to failure of the sample). No anisotropic behaviour is seen in the equiaxial test because the value of stress in both x and y directions are almost the same (Fig. 19b). A 2D local strain distribution of $\varepsilon_{xx}$, $\varepsilon_{yy}$, $\varepsilon_{xy}$ in various biaxial deformations at $E_y = 0.2$ is shown in Fig. 19c. A uniform local strain distribution is achieved throughout the surface other than

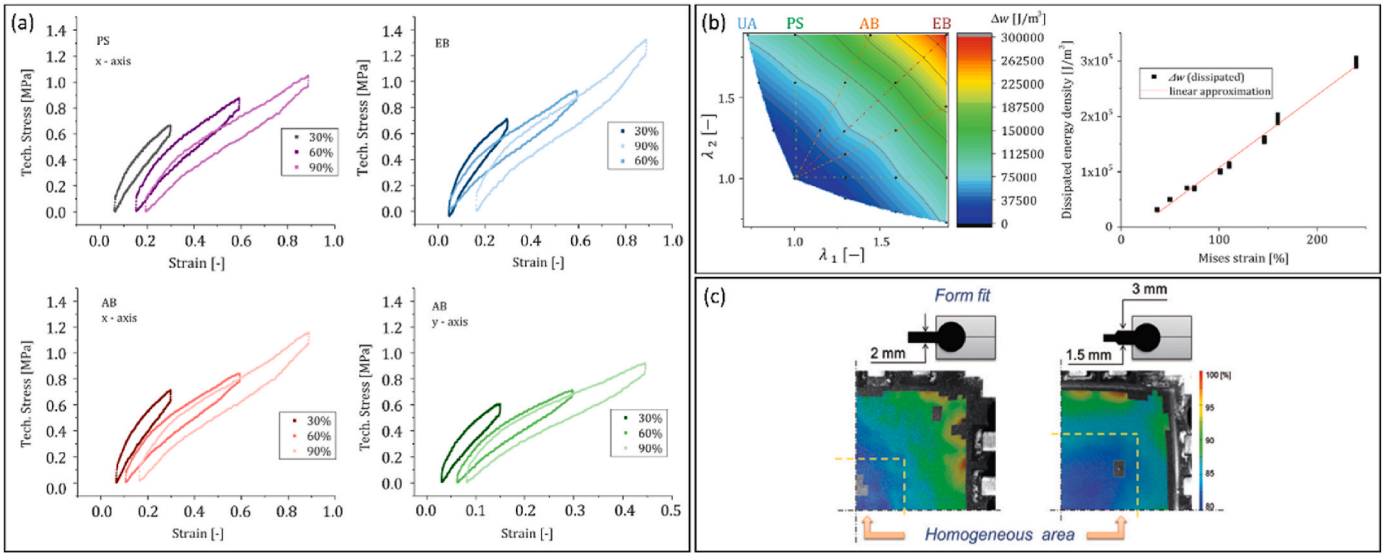


**Fig. 14.** Biaxial tension of SBR filled CB: (a) stress-strain curve at cycle #300 (b) energy dissipation at different loading conditions. [131], *(c) different clamping systems composed of a bulge shape at the edge to reach bigger region of homogeneity in the middle* [132].

the vicinity of the edges. Most importantly, the local strain distribution within the surface is equal to imposed strain (nominal strain) without the presence of shear strain, i.e., $\varepsilon_{xx} = Ex$, $\varepsilon_{yy} = Ey$, $\varepsilon_{xy} = 0$.

Fig. 19d shows the force-displacement plot up to failure (imposed displacement) of a single edge notched samples with various initial lengths in the range of −10 to +10 mm subjected to different biaxial loadings. The force perpendicular to the notch length ($F_y$) substantially decreases with an increase in $X_c$ whereas the force along the notch direction ($F_x$) is less affected by an increase in $X_c$. It is worth noting that the notch opening increases by displacement increase, though no propagation takes place until macroscopic failure as shown by the crossmarks in Fig. 19 d. Similar to the sample without a notch, $F_y$ for the EB sample was larger, followed by UB and PE samples, respectively.

Two different approaches were used to obtain strain energy release rate. The first one is done by biaxial loading of single edge notch sample with varied initial notch lengths ($X_c$) while equation (19) was used for the calculation:

$$G(E_x, E_y) = \frac{1}{t}\left[\frac{dW(X_c, U_x, U_y)}{dX_c}\right]_{U_x, U_y}, \tag{19}$$

in which G is the strain energy release rate, W is the strain energy, $X_c$ is the initial notch length, $U_x$ and $U_y$ are imposed displacements in x and y directions, respectively and t is the sample thickness. The strain energy was obtained from the integrated area of force-displacement in Fig. 19d using equation (20) as shown in the inset of Fig. 19e:

$$W = W_x + W_y = \int F_x dU_x + \int F_y dU_y \tag{20}$$

It can be concluded that regardless of the deformation state, the strain energy at the same $U_x$ and $U_y$ is decreased with the increase of $X_c$; besides, it is increased when imposed displacement increase (at the same notch length). Finally, the W-$X_c$ relation can be approximated by linear regression of the curve in Fig. 19e, thus, $\frac{dW}{dX_c}$ at different $U_x$ *and* $U_y$ can be obtained from the slope.

The other method used in their study to measure stress energy release rate was based on the strain energy differences between two different deformations. One is biaxial loading of the sample without any notch as shown in Fig. 19b and the other one is a uniaxial tensile test in which one edge is constrained and the other one is loose as shown in the inset of Fig. 19f. This represents the condition of the specimen right after crack passage called Residual Extension (RE). The dimension of the RE sample was 65 × 32.5 $mm^2$ i.e. half of the original sample. The difference in the strain energy density amongst two states denoted as ΔA was obtained using equation (21):

$$\Delta A(E_x, E_y) = A(E_x, E_y) - A_{RE}(E_x) \tag{21}$$

where $A(E_x, E_y)$ and $A_{RE}(E_x)$ are the strain energy densities for biaxial loading without notch and RE sample, respectively. $A(E_x, E_y)$ and $A_{RE}(E_x)$ can be obtained from $\sigma_i$–$E_i$ (i = x and y) and $\sigma_x$–$E_x$ for biaxial and RE samples, respectively, using equation (22)–(23), respectively. The $A_{RE}$ for PE sample was zero as there is no strain at this direction.

$$A(E_x, E_y) = A_x + A_x = \int \sigma_x dE_x + \int \sigma_y dE_y \tag{22}$$

$$A_{RE} = \int \sigma_x dE_x \tag{23}$$

The $\Delta A - E_y$ curves for different deformation states are shown in Fig. 19f indicating larger $\Delta A$ for the EB sample, followed by UB and PE, respectively. Finally, the ratio of strain energy release rate and initial length in y-direction ($L_{0,y}$) is equal to $\Delta A$ (equation (24)) indicating that two methods reach to a similar strain energy release rate as shown in Fig. 19f. It can be concluded that the strain energy release rate in the biaxial states can be accurately obtained using a simpler approach by two different biaxial loading states without any notches rather than laborious approaches of making various notches. This remarkable finding in measuring energy release rate using a cost-effective and user-friendly approach need to be further investigated for other soft materials so that it can be extended as robust and versatile technique for fracture toughness measurement in viscoelastic materials.

$$\frac{G(E_x, E_y)}{L_{0,y}} = \Delta A(E_x, E_y) = A(E_x, E_y) - A_{RE}(E_x) \tag{24}$$

In summary, as listed in Table 1 and briefly reviewed in this section, different test parameters including strain rate, strain amplitude, pre-stretch, pre-crack length were used for viscoelastic and fracture characterization of soft materials in biaxial modes. This necessitates importance of writing a guideline for biaxial characterizations of soft materials in which few agenda will be suggested in section 6 by taking into account the previous works performed on biaxial characterizations.

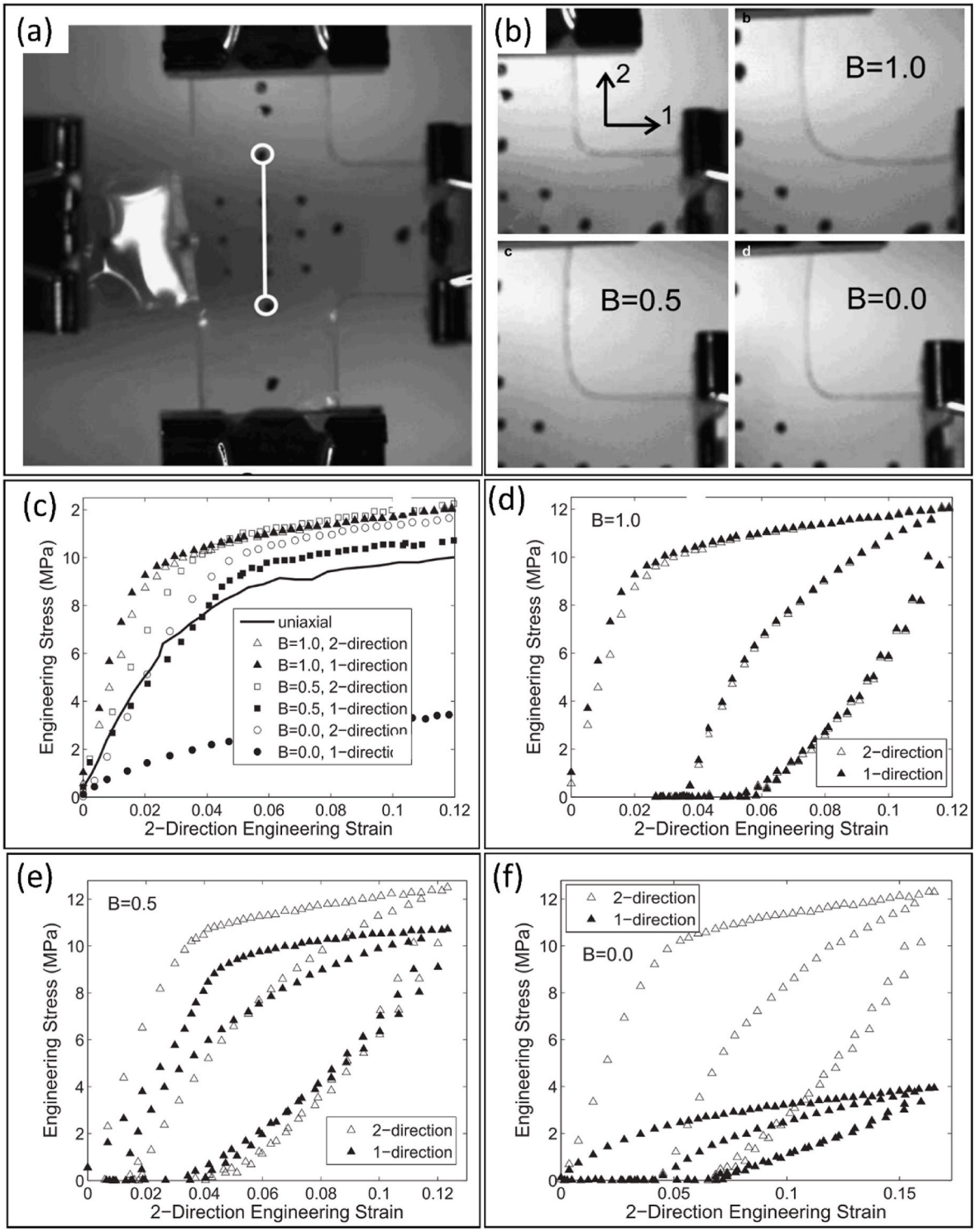


**Fig. 15.** Biaxial characterizations of Nafion membrane: (a) measurement of local strain in biaxial test, (b) comparison of undeformed and deformed sample during different biaxial loadings, true stress-true strain curves (c) different biaxial tests under monotonic loading, (d) equi-biaxial loading under cyclic loading, (e) cyclic biaxial loading with the strain rate twice in one direction with respect to other direction, (f) cyclic biaxial loading with one direction fixed [83].

## 5. Inflation test

The previous sections were focused on biaxial characterization using square or cruciform samples. However, inflation, bubble or bulge test is also one of the most common equibiaxial tests performed on elastomers [62,63,67,134–139]. It is employed to examine hyperelastic and viscoelastic properties of various polymers [140]. It is well addressed in the literature that the strain field distribution near the edges are planar tension whereas the one in the vicinity of the pole are mostly equibiaxial [141,142]. It was first discussed by Treloar et al. [143] in which a vulcanized latex behavior and its model parameters were investigated. Likewise, this test was also used for biological human tissues to explore the aneurysms under biaxial strain and stress fields, and to characterize viscoelastic properties of human tissues [144,145].A brief review will be

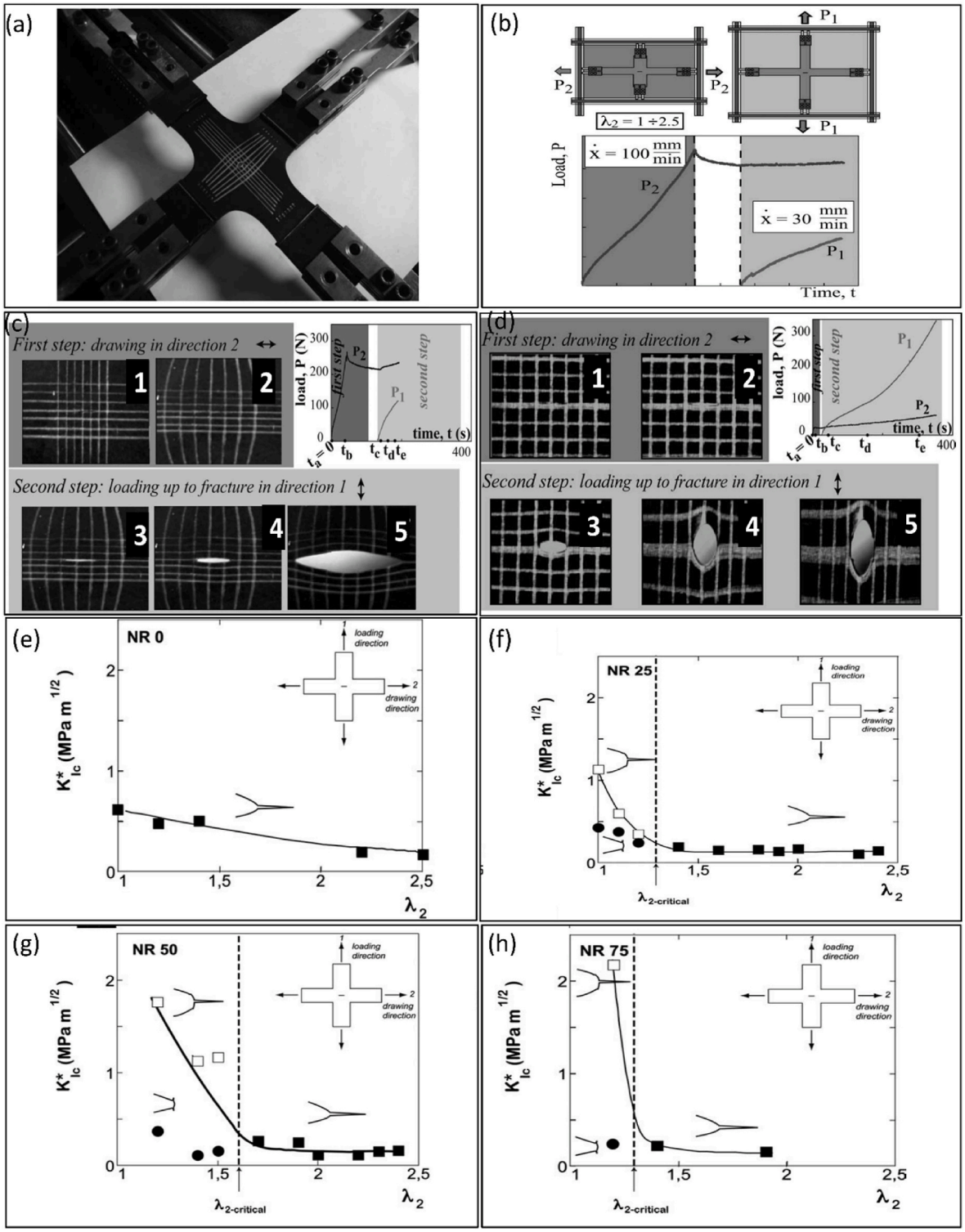


**Fig. 16.** (a) Cruciform specimen with a pre-crack, (b) experimental setup, (c–d) frames of video taken during the fracture test from NR75 at $\lambda_2 = 1.9$ and NR50 ($\lambda_2 = 1.2$), respectively, (e–h) $K_{IC}$ - $\lambda_2$ for NR, NR25, NR50, and NR 75, respectively, in which full squares and full circles highlight the onset of a forward crack only and the onset of sideways cracks followed by a forward crack (open square), respectively. Numbers 1 to 5 in (c–d) show steps of the test in the order [71].

conducted throughout this section to better understand the sample configurations and test setups for the bulge test.

Sasso et al. [67]. studied properties of a hyperelastic rubber using uniaxial and biaxial tensile tests. Afterwards, they fitted the experimental data with some hyperelastic constitutive models including Mooney–Rivlin (first and second order), Ogden, Yeoh, neo-Hookean, Arruda–Boyce. For the biaxial test, a bulge test was conducted as shown in Fig. 20a by holding a thin disc of rubber using two flanges and inflated by pumping liquid into the flange orifice so that the specimen became a balloon-like shape. A very low strain rate of $2 \times 10^{-3}\ s^{-1}$ was employed to avoid viscous behaviour of the rubber. Uniaxial test manifested quite a larger elastic deformation at the same stress with respect to a biaxial test (Fig. 20b). The fitting of different models with uniaxial and biaxial tests are also plotted in Fig. 20c and d, respectively.

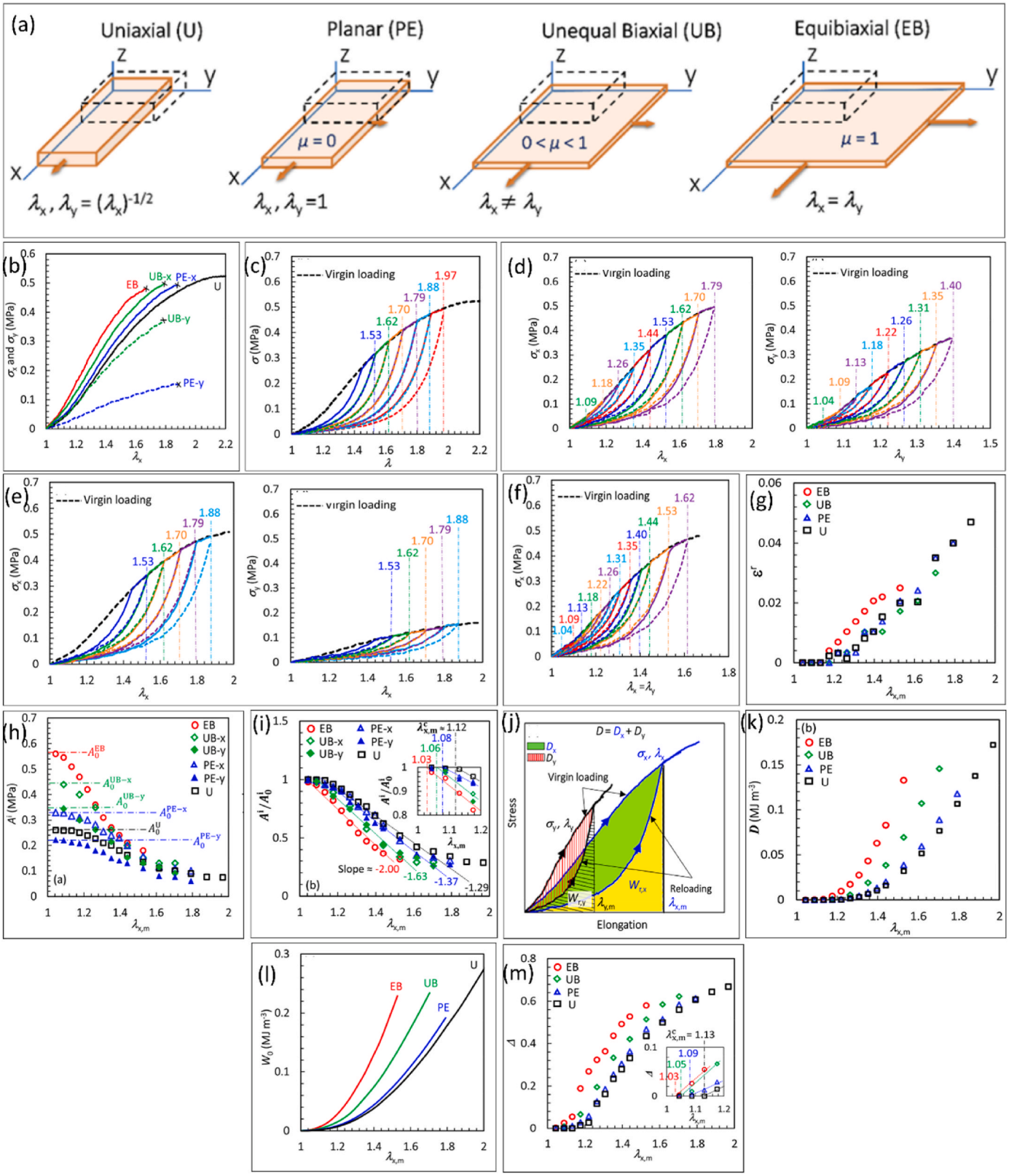


**Fig. 17.** Uniaxial and biaxial characteristics of hydrogel: (a) various loading conditions, (b) nominal stress-strain curve in quasi-static condition, (c–f) nominal stress-strain curve at loading-unloading cycles for U, PE, UB, and EB respectively, (g) residual strain versus stretch ratio, (h) Initial elastic modulus ($A^i$) versus stretch ratio, (i) ratio of initial modulus to virgin loading-unloading at one complete cycle with respect to stretch ratio, (j) illustration of the input energy and dissipation energy at first loading-unloading of EB, (k–m) dissipation, input work and dissipation factor for virgin loading loading-unloading, respectively [79].

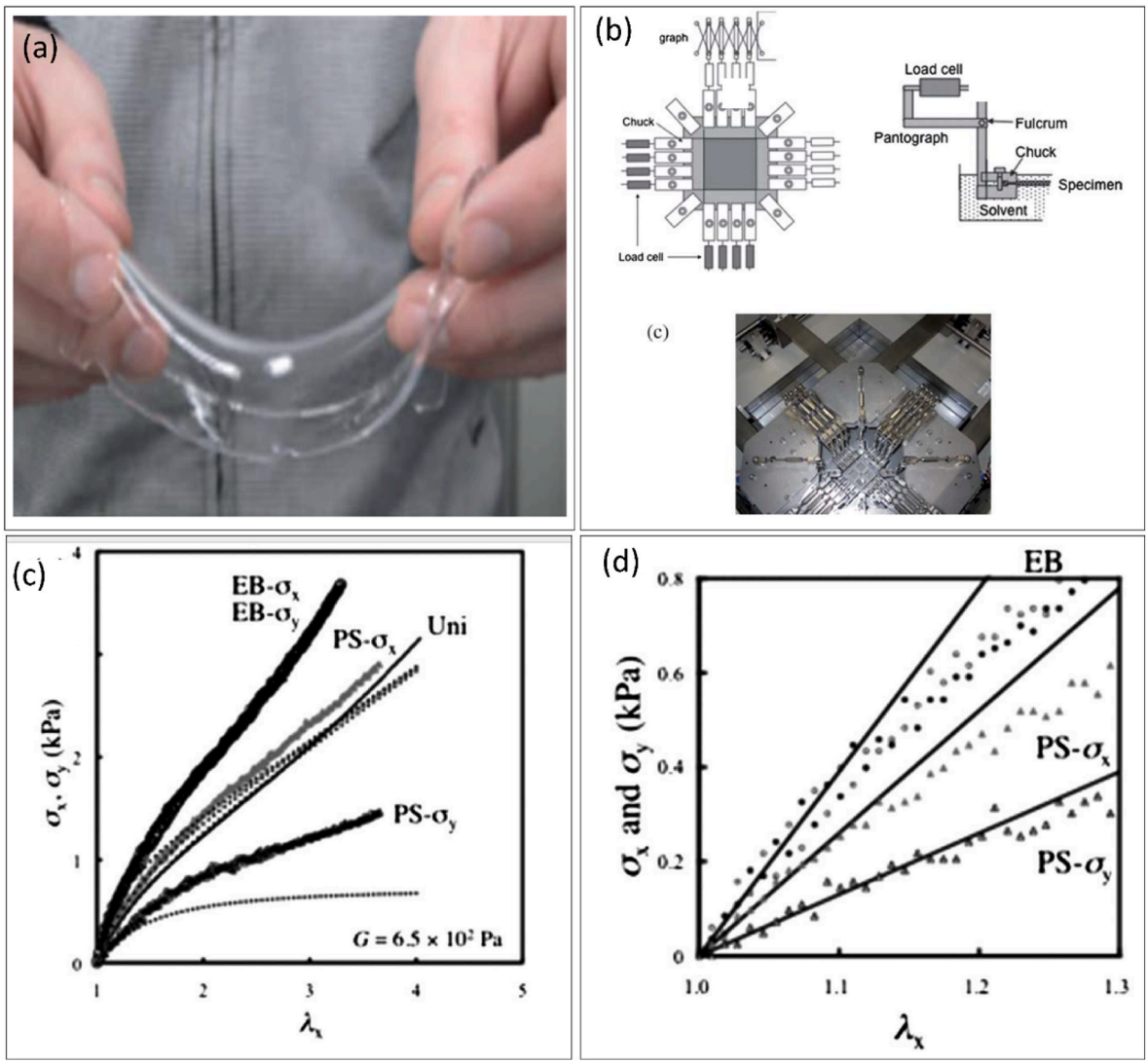


**Fig. 18.** Biaxial characterization of soft polymer gel, PAAm-CG-2: (a) deflecting of the sample by its own weight, (b) biaxial setup in a solvent bath, (c) stress-strain curve in different loading conditions, (d) stress-stress curve in $\lambda < 1.3$ [84].

According to their results, Ogden and Mooney– Rivlin models manifested the best fitting with the experimental data in both uniaxial and biaxial data, though the latter manifested higher RMS (Root Mean Square). Unlike to proper fitting of Ogden and Mooney– Rivlin models reported by them [67], the aforementioned numerical models failed to reproduce the inflation-jump and limit-point instabilities [146,147] in incompressible materials during inflation test. Indeed, these variations in fitting experimental datasets with existing hyperelastic models can be attributed to either lack of robust standardized protocol for experimental characterizations of the elastomers including biaxial modes or different invariants used in each hyperelastic models. In other words, some models can be well fitted with the uniaxial experiments whereas they fail to capture the deformation in a more complex loading conditions including biaxial and inflation tests. This again shows the importance of preparing a standardized protocol for biaxial characterizations of elastomers which can help to develop a versatile and comprehensive hyperelastic model for incompressible materials.

Similar to unfilled elastomers, biaxial fatigue properties of filled elastomers such as magnetorheological elastomers (MREs) (a silicone rubber filled with carbonyl iron particles up to 20 vol %), were studied using a bubble inflation method [134]. The samples for the fatigue test were a disk with 50 mm diameter and 1 mm thickness. This experimental setup (Fig. 21a) can reduce the drawback of stretching specimens by the grips, thus, hindering stress concentration in the clamping region. For the fatigue tests, different stress amplitudes ranging from $\sigma_a = 0.75$ MPa to $\sigma_a = 1.4$ MPa with a minimum stress of zero and stress ratio of $R = 0$ were utilized (Fig. 21b). Quasi-static tensile strengths of 3.5 MPa and 4.1 MPa were achieved for the isotropic and anisotropic specimens, respectively. A common "S" type stress -strain curve was observed for both samples at $\sigma_a = 0.75$ MPa at different cycles as shown in Fig. 21c–d. In addition, hysteresis and stress softening effect were also noted, especially at the cycles less than 100. Finally, an induced permanent set resulting from the cyclic loading was noted throughout the progressive cyclic loading, though the increase was more pronounced in the isotropic specimen compared to the anisotropic one indicating higher elongation in the former and less stiffness with respect to the latter.

Xu et al. [137], studied the effects of different fillers such as Graphene Oxide (GO) and Carbon Nanotubes(CNTs) on biaxial fatigue properties of SBR elastomer using an inflation test (Fig. 22). Hysteresis effect can be clearly seen for all composites resulting from viscoelastic properties of the SBR. As it is shown in Fig. 22a–c, the hysteresis can still occur at high cycles when samples are subjected to biaxial fatigue loading. In other words, the fillers change their structures and orientations continuously throughout this type of loading condition. Likewise, the hysteresis area of hybrid SBR composites is higher than the binary resulting in more dissipation of energy in the former composite. Finally,

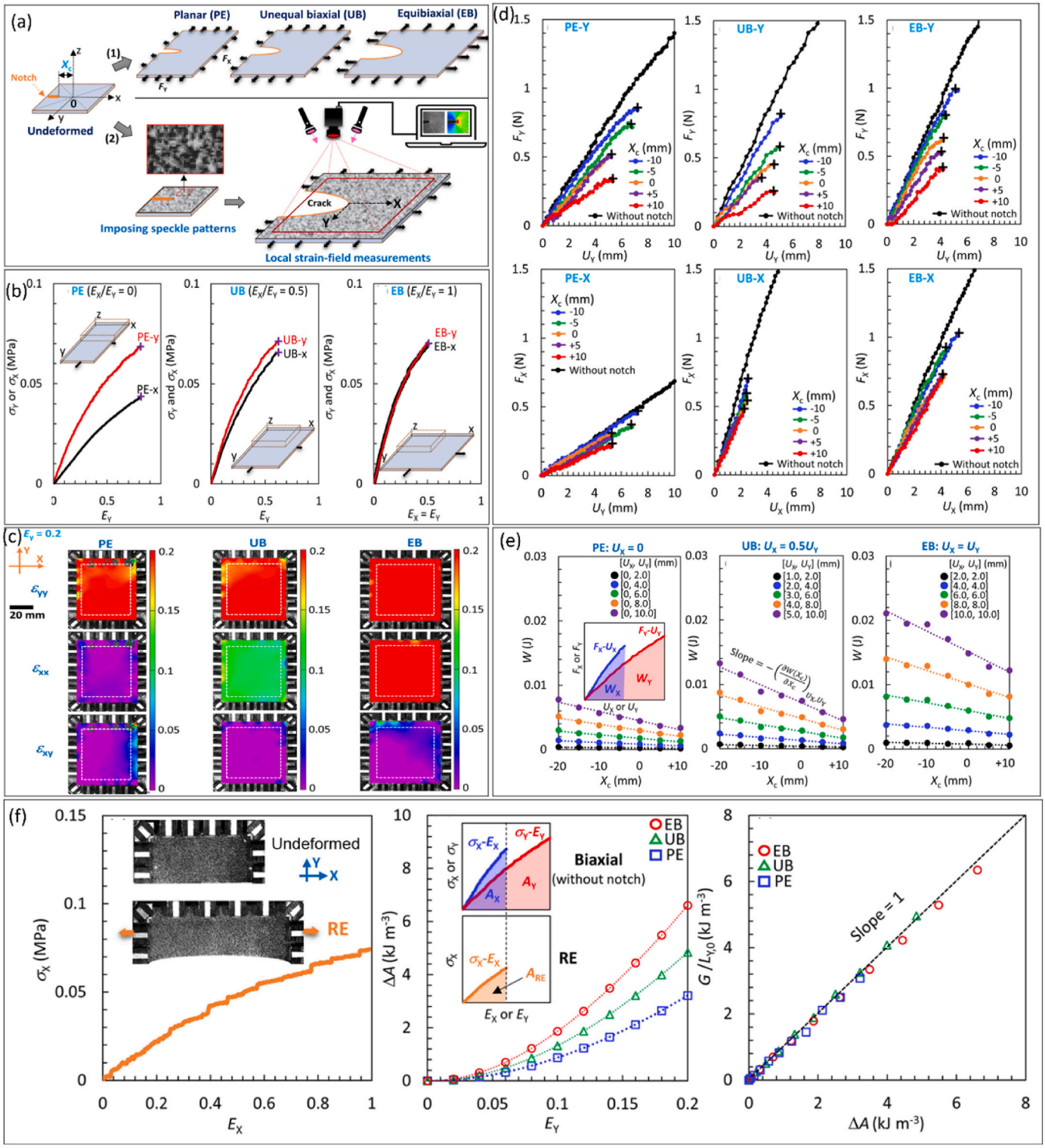


**Fig. 19.** Biaxial characterization of PDMA hydrogel: (a) different biaxial deformations of single edge notched specimen, (b) nominal stress-nominal strain curves of the sample without notch, (c) 2D local strain distribution at $E_y = 0.2$ (d) tensile force-imposed displacement for the single-edge notched specimens, (e) strain energy versus initial notch length, (f) calculation of strain energy release rate using uniaxial tensile test where one edge is constrained and the other one is loose [85].

the S–N curve presented in Fig. 22d indicates higher fatigue life for GO-$SiO_2$/SBR > CNT-$SiO_2$/SBR > $SiO_2$/SBR, respectively, under the same stress amplitude while it decreases by increasing stress amplitudes.

## 6. Future works

Significant variations in terms of materials, sample dimensions and configurations along with various test setups including strain rate, pre-stretching, clamping systems were found in the literature for the biaxial test (Table 1). Indeed, it is hard to compare the results together

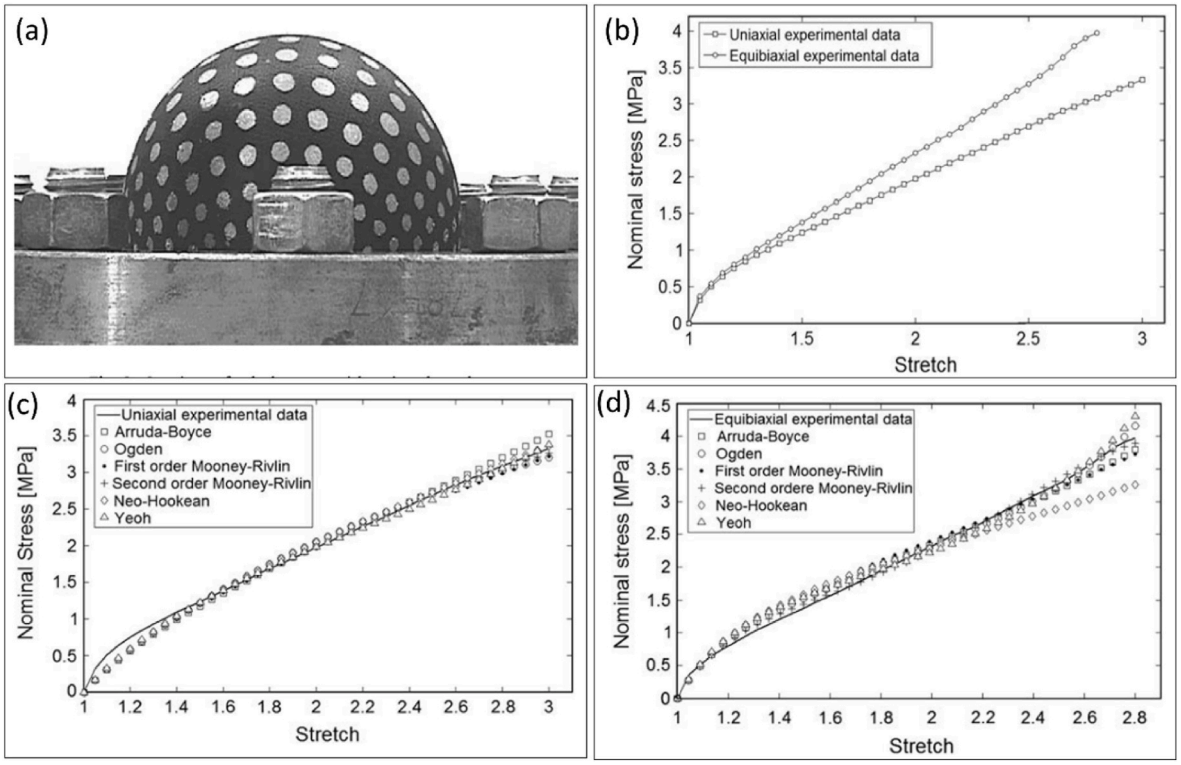


**Fig. 20.** Uniaxial and biaxial tension characterizations of a hyperelastic rubber: (a) bulge test setup, (b) experimental uniaxial and biaxial tensile test results, (c–d) fitting uniaxial and biaxial tests with different constitutive models respectively [67].

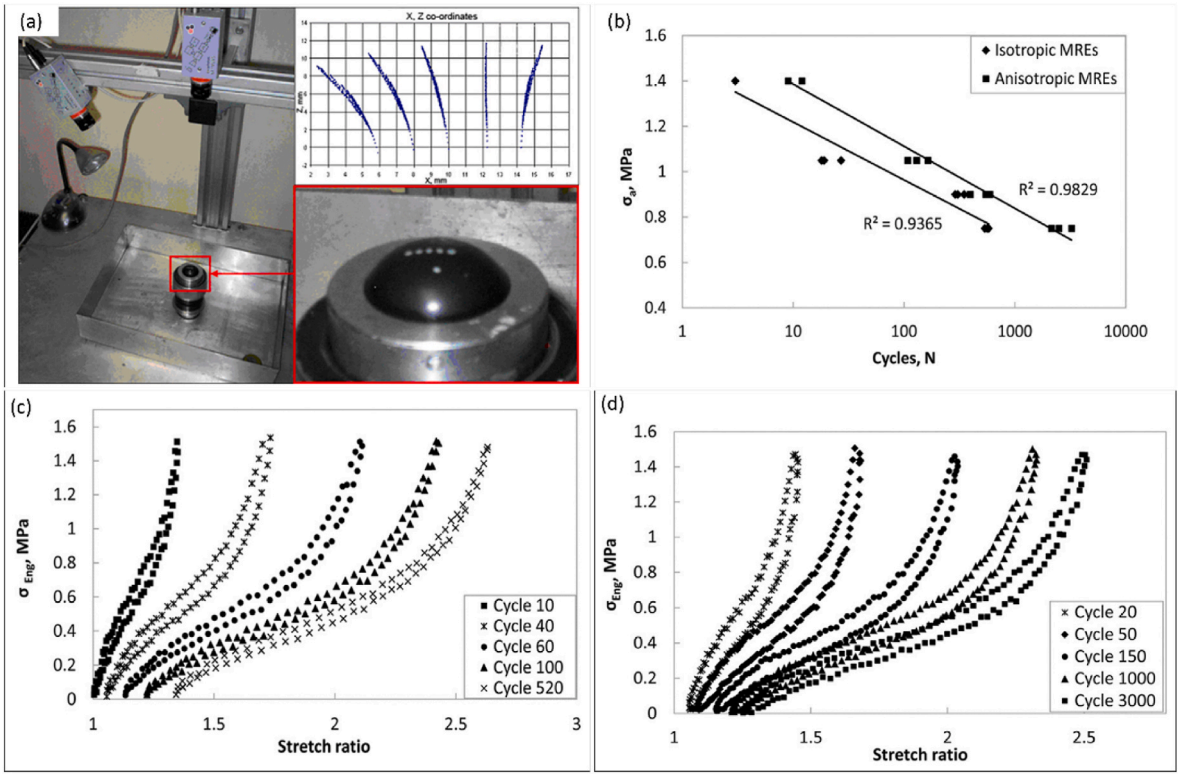


**Fig. 21.** Biaxial fatigue test of MREs composites: (a) bubble inflation method, (b) S–N curve, (c–d) stress-strain curve $\sigma_a = 0.75$ MPa for isotropic and anisotropic samples respectively [134].

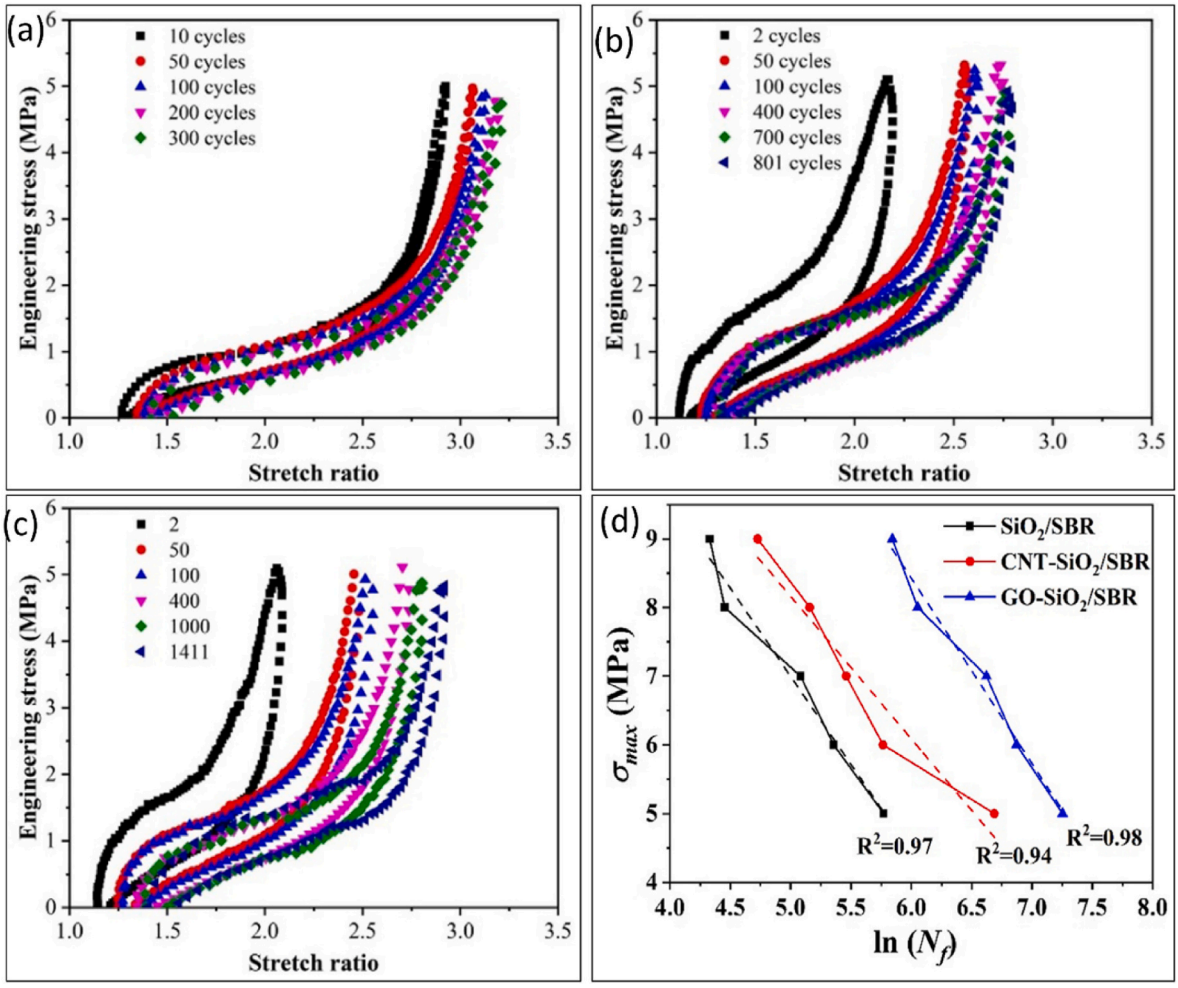


**Fig. 22.** (a–c) Stress-strain curve of equibiaxial fatigue test at different cycles for $SiO_2$/SBR, CNT-$SiO_2$/SBR, and GO-$SiO_2$/SBR, respectively, (d) S–N curve [137].

due to lack of consensus amongst the research communities and the absence of a standardized protocol for the biaxial charaterization. This becomes more significant as many elastomers are subjected to biaxial loading in their service life, thus, it is of importance to establish a new standard in which a good agreement can be met amongst scientists and engineers. Although a wide range of biaxial tests were already well established for metallic materials [148], no standard or test procedure was adopted for soft polymers where experimental study through biaxial tension test is of significant importance for developing proper understanding of polymer properties as well as achieving high-fidelity hyperplastic constitutive models. A few preliminary studies were conducted on biaxial test setups and sample optimization [149,150], however it is hard to conclude which sample geometry and test setup should be used for soft polymers. For example, Chretien et al. [149] mostly discussed a biaxial tension rig as well as gripping mechanism designed for soft tissues while a very small square samples (25 × 25 $mm^2$) was used. Pini et al. [150] performed a comprehensive study on cruciform sample optimization by comparing their designs (G1 and G2 design as shown in Fig. 23 a-b, respectively) with types A and D shown in Fig. 3c that suggested in Ref. [73]. They indicated that both geometries could reach proper biaxiality, but the G2 manifested higher strain in the middle with less reliability.

Therefore, we suggest that a comprehensive study shall be done using different materials such as natural rubbers, silicone rubbers, acrylics, polyurethanes, hydrogels, etc while at least three different cruciform geometries must be used as shown in Fig. 23. It is worth noting that the clamping system of square samples is quite more complex with respect to the cruciform samples, especially for the cyclic loading tests; thus, making it more expensive test compared with a cruciform sample. We believe that the best optimization for the biaxial cruciform specimens were performed by Refs. [73,75,76], though different configurations was used. Therefore, it is worth comparing these three geometries (Fig. 23c–e) at different test parameters while using various soft polymeric materials. This should be done at least in three different strain rates i.e. 0.01 $s^{-1}$, 0.05 $s^{-1}$ and 0.1 $s^{-1}$ and several strain amplitudes ranging from 50 % to 200 % with 50 % interval. This would provide a better understanding of the distribution of biaxial strain within the region of interest (i.e., in the middle of a cruciform sample) as well as achieving the higher strain in the middle. In other words, amongst the three suggested designs, the one with proper biaxiality degree based on equations (1)–(3), can be an ideal configuration for any biaxial tension test. This can be further validated using numerical analysis by fitting a proper viscoelastic model into the experimental results.

In addition, additional thickening needs to be performed for the suggest configurations to achieve maximum strain in the middle while equations (2) and (3) shall be met. This is done to avoid reaching maximum strain in the arm, which leads to final failure within the arm. Therefore, gauge section reduction of the cruciform sample shall be done like the works illustrated in Fig. 24a–b. Same concepts shall be applied to the square samples as shown in Fig. 24c. The thickness reduction in the gauge section or edge thickening for both cruciform and square specimens are critical i.e. not only to achieving proper biaxially, but also to avoid stress concentration arisen from the grips. Fig. 24d–f illustrate the extra stress imposed on the sample edge which resulted in

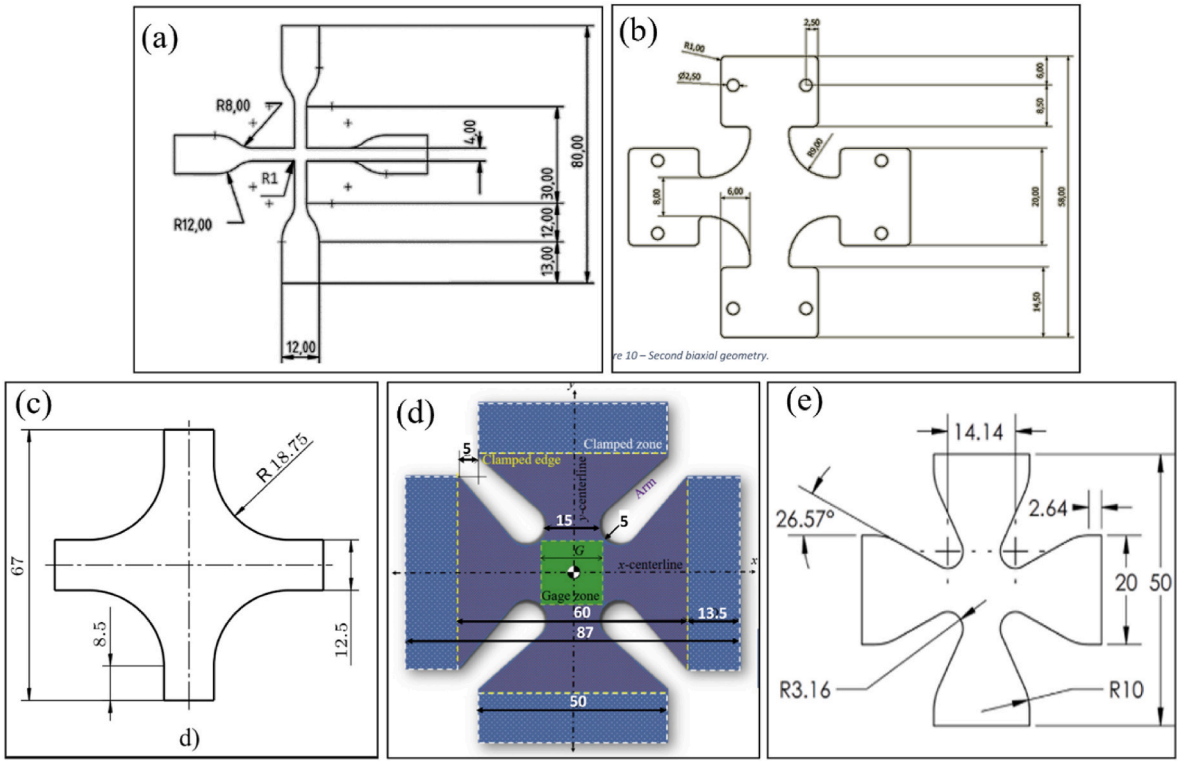


**Fig. 23.** (a–b) Two different geometry developed in Ref. [150] *which were further modified based on type A and D in Ref.* [73] *respectively,(c-e) three suggested sample configurations for future experimental and numerical investigations: (c)* [73], *(d)* [75],*(e)* [76].

failure of the samples in vicinity of the gripping region during cyclic biaxial test which is shown by red arrows. It is worth noting that the cyclic biaxial fatigue tests represented in Fig. 24d–h are currently running in our lab to better explore the geometrical and gripping effects on running proper biaxial test and to provide better guidelines for future investigations.

## 7. Conclusion

This review paper was aimed to investigate biaxial properties of soft polymers. Very limited works were conducted on biaxial characteristics of soft polymers since it is a challenging and expensive test procedure. Due to lack of specific test protocol for the biaxial characterization of soft polymers, significant variations were observed in the literature in terms of sample dimension and configuration, testing protocol, and gripping systems. Therefore, a comparison of different studies was done in this review in terms of sample shape and dimension, and biaxial test methodology. The following conclusions can be drawn:

- High variations in terms of shape and dimension of the samples were seen in which the smallest and largest cruciform samples with the dimensions of 38 × 38 mm and 165 × 165 mm were used, respectively, while a minimum sample of 7 × 7 mm and maximum of 70 × 70 mm were used for the square specimen. It is quite difficult to identify which configuration is optimum for the biaxial test as various materials and loading scenarios were used. This necessitates the importance of preparing new protocol for biaxial characterization for soft polymers based on the testing materials and applications.
- Many optimization approaches were performed to find out an optimum shape of cruciform sample in reaching highest biaxiality degree. It was noted that the clamping mechanism for square samples was more complex than the cruciform samples, especially for cyclic loading; thus, made it a more expensive configuration for biaxial testing. We believed that the best optimization of biaxial cruciform sample were done by Refs. [73,75,76], although different configurations was used.
- Equations (1)–(3) were defined for proper biaxiality in which a perfect biaxiality means that the principal strains in the center of the sample, $E^c_{xx}$ and $E^c_{yy}$ , should be equal, thus, test function $\Gamma(x,y)$ (equation (1)) demonstrated the variations from perfect biaxiality in the region of interest i.e. the more $\Gamma(x,y)$ the more uniaxiality and vice versa. In addition, the uniaxial strain in the arms was much higher than the middle area for a cruciform sample i.e. $E^{(x,y)}_{xx} \gg E^c_{xx}$ and $E^{(x,y)}_{yy} \gg E^c_{yy}$ , thus, a new factor was taken into account to define Degree of Efficiency (DOE) (equation (2)) demonstrating the strain discrepancy between the arm and the center region.
- Various loading conditions including EB, UB, PS were used while various strain amplitudes and strain rates were employed. In addition, different pre-stretching values and gripping systems were also used to smoothen the effects of grips to avoid either slipping from the grips or sample failure in the vicinity of the grips due to large stress concentration induced. In this context, several techniques were suggested including reinforcing the edge by gluing two pieces on both sides or thickening the edges by moulding if the sample should be one piece. This would help to increase the biaxial strain of the middle area of cruciform sample without any failure from the grips.
- Three cruciform geometries were suggested for future investigation to be tested with different test parameters and different materials. It was recommended to use at least three different strain rates, i.e. 0.01 $s^{-1}$, 0.05 $s^{-1}$ and 1 $s^{-1}$ and several strain amplitudes ranged from 50% to 200 % with 50 % interval. This resulted in a better grasping of strain distribution within the region of interest and subsequently the status of proper biaxiality.
- Apart from the suggest geometries, gauge reduction or edge thickening should be considered on both cruciform and square geometries to achieve better biaxiality and to avoid stress concentration induced by the grips. This was of vital importance to conduct reliable biaxial

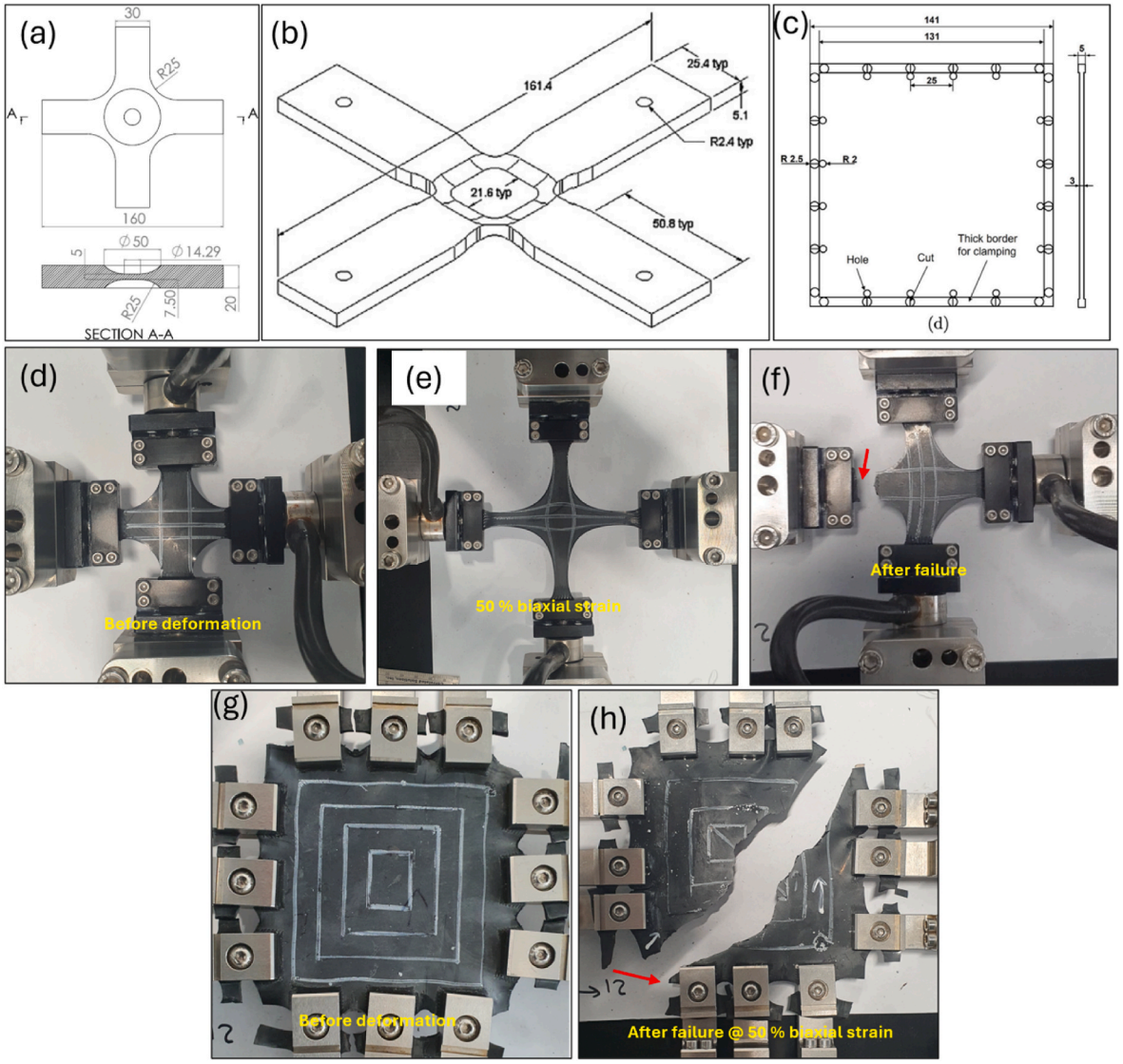


**Fig. 24.** (a–b) Various gauge reductions for the cruciform samples developed by Refs. [91,93], *respectively, (c) edge thickening performed on square sample* [117], *(d-f) ongoing cyclic biaxial tests on cruciform sample conceptualized based on type D geometry suggested by Seibert* et al. [73], *(g-h) our ongoing cyclic biaxial tests on square samples.*

test, for high cyclic conditions; otherwise, biaxial test performed on samples with uniform thickness resulted in uniaxial failure rather than biaxial.

## Author statement

Ali Esmaeili: Initial Draft Writing, Data Analysis, Editing, Deepak George: Editing and improvements of Initial Draft, Ian Masters: Editing, Analysis and Draft writing, Mokarram Hossain: Conceptualisation, Grant Management, Draft Writing and Editing.

## Declaration of competing Interest

The authors declare that they have no known competing financial interests or personal relationships that could have appeared to influence the work reported in this paper.

## Data availability

Data will be made available on request.

## Acknowledgements

This study is funded by the Swansea Bay City Deal and the European Regional Development Fund through the Welsh European Funding Office. This study is also supported by EPSRC through the Supergen ORE Hub (EP/S000747/1), who have been awarded funding for the Flexible Fund project Submerged bi-axial fatigue analysis for flexible membrane Wave Energy Converters (FF2021-1036).

## References

[1] A.V. Kaliyathan, A.V. Rane, K. Kanny, H.J. Maria, S. Thomas, Thermoplastic Elastomers for Shock Absorbing Application, Elsevier Ltd., 2022, https://doi.org/10.1016/b978-0-12-820352-1.00196-6.
[2] X.H. Long, Y.T. Ma, R. Yue, J. Fan, Experimental study on impact behaviors of rubber shock absorbers, Construct. Build. Mater. 173 (2018) 718–729, https://doi.org/10.1016/j.conbuildmat.2018.04.077.
[3] A. Bera, D. Ganguly, S.K. Ghorai, J.P. Rath, S. Ramakrishnan, J. Kuriakose, S.K. P. Amarnath, S. Chattopadhyay, Treatment of natural rubber with bio-based components: a green endeavor to diminish the silica agglomeration for tyre tread application, Chem. Eng. J. Adv. 11 (2022), 100349, https://doi.org/10.1016/j.ceja.2022.100349.
[4] L. Ma, Y. Zhai, C. Wan, Z. Zhang, C. Zhang, S. Wang, Efficient thermo-oxidative reclamation of green tire rubber and silanized-silica/rubber interface

characterization, Polym. Degrad. Stabil. 196 (2022), https://doi.org/10.1016/j.polymdegradstab.2022.109827.
[5] C. Porter, B. Zaman, R. Pazur, A critical examination of the shelf life of nitrile rubber O-Rings used in aerospace sealing applications, Polym. Degrad. Stabil. 206 (2022), 110199, https://doi.org/10.1016/j.polymdegradstab.2022.110199.
[6] H. Chang, Z. Wan, X. Chen, J. Wan, L. Luo, H. Zhang, S. Shu, Z. Tu, Temperature and humidity effect on aging of silicone rubbers as sealing materials for proton exchange membrane fuel cell applications, Appl. Therm. Eng. 104 (2016) 472–478, https://doi.org/10.1016/j.applthermaleng.2016.05.095.
[7] I. Collins, M. Hossain, W. Dettmer, I. Masters, Flexible membrane structures for wave energy harvesting: a review of the developments, materials and computational modelling approaches, Renew. Sustain. Energy Rev. 151 (2021), 111478, https://doi.org/10.1016/j.rser.2021.111478.
[8] G. Moretti, M. Santos Herran, D. Forehand, M. Alves, H. Jeffrey, R. Vertechy, M. Fontana, Advances in the development of dielectric elastomer generators for wave energy conversion, Renew. Sustain. Energy Rev. 117 (2020), 109430, https://doi.org/10.1016/j.rser.2019.109430.
[9] G. Moretti, G.P.R. Papini, M. Righi, D. Forehand, D. Ingram, R. Vertechy, M. Fontana, Resonant wave energy harvester based on dielectric elastomer generator, Smart Mater. Struct. 27 (2018), https://doi.org/10.1088/1361-665X/aaab1e.
[10] G. Moretti, G.P.R. Papini, L. Daniele, D. Forehand, D. Ingram, R. Vertechy, M. Fontana, Modelling and testing of a wave energy converter based on dielectric elastomer generators, Proc. R. Soc. A Math. Phys. Eng. Sci. 475 (2019), https://doi.org/10.1098/rspa.2018.0566.
[11] S. Chiba, M. Waki, T. Wada, Y. Hirakawa, K. Masuda, T. Ikoma, Consistent ocean wave energy harvesting using electroactive polymer (dielectric elastomer) artificial muscle generators, Appl. Energy 104 (2013) 497–502, https://doi.org/10.1016/j.apenergy.2012.10.052.
[12] A. Sasmal, A. Arockiarajan, Recent progress in flexible magnetoelectric composites and devices for next generation wearable electronics, Nano Energy 115 (2023), 108733, https://doi.org/10.1016/j.nanoen.2023.108733.
[13] Q. Gao, S. Agarwal, A. Greiner, T. Zhang, Electrospun fiber-based flexible electronics: fiber fabrication, device platform, functionality integration and applications, Prog. Mater. Sci. 137 (2023), 101139, https://doi.org/10.1016/j.pmatsci.2023.101139.
[14] Q. Wei, J. Zhou, Y. An, M. Li, J. Zhang, S. Yang, Modification, 3D printing process and application of sodium alginate based hydrogels in soft tissue engineering: a review, Int. J. Biol. Macromol. 232 (2023), 123450, https://doi.org/10.1016/j.ijbiomac.2023.123450.
[15] R. Yang, R. Wang, S. Abbaspoor, M. Rajan, A. Turki Jalil, M. Mahmood Saleh, W. Wang, In vitro and in vivo evaluation of hydrogel-based scaffold for bone tissue engineering application, Arab. J. Chem. 16 (2023), 104799, https://doi.org/10.1016/j.arabjc.2023.104799.
[16] M. Cianchetti, C. Laschi, A. Menciassi, P. Dario, Biomedical applications of soft robotics, Nat. Rev. Mater. 3 (2018) 143–153, https://doi.org/10.1038/s41578-018-0022-y.
[17] D. Rus, M.T. Tolley, Design, fabrication and control of soft robots, Nature 521 (2015) 467–475, https://doi.org/10.1038/nature14543.
[18] S. Terryn, J. Langenbach, E. Roels, J. Brancart, C. Bakkali-Hassani, Q.A. Poutrel, A. Georgopoulou, T. George Thuruthel, A. Safaei, P. Ferrentino, T. Sebastian, S. Norvez, F. Iida, A.W. Bosman, F. Tournilhac, F. Clemens, G. Van Assche, B. Vanderborght, A review on self-healing polymers for soft robotics, Mater. Today 47 (2021) 187–205, https://doi.org/10.1016/j.mattod.2021.01.009.
[19] L.Y. Zhou, J. Fu, Y. He, A review of 3D printing technologies for soft polymer materials, Adv. Funct. Mater. 30 (2020), https://doi.org/10.1002/adfm.202000187.
[20] V. Gupta, S. Gupta, A. Chanda, Development of an ultra-low-cost planar biaxial tester for soft tissue characterization, Biomed. Phys. Eng. Express. 9 (2023), https://doi.org/10.1088/2057-1976/acb940.
[21] S.D. Waldman, J.M. Lee, Effect of sample geometry on the apparent biaxial mechanical behaviour of planar connective tissues, Biomaterials 26 (2005) 7504–7513, https://doi.org/10.1016/j.biomaterials.2005.05.056.
[22] W. Sun, M.S. Sacks, M.J. Scott, Effects of boundary conditions on the estimation of the planar biaxial mechanical properties of soft tissues, J. Biomech. Eng. 127 (2005) 709–715, https://doi.org/10.1115/1.1933931.
[23] S.D. Waldman, M.S. Sacks, J.M. Lee, Boundary conditions during biaxial testing of planar connective tissues Part II Fiber orientation, J. Mater. Sci. Lett. 21 (2002) 1215–1221.
[24] S.D. Waldman, J. Michael Lee, Boundary conditions during biaxial testing of planar connective tissues. Part 1: dynamic behavior, J. Mater. Sci. Mater. Med. 13 (2002) 933–938, https://doi.org/10.1023/A:1019896210320.
[25] V. Gupta, S. Gupta, A. Chanda, Development of an ultra-low-cost planar biaxial tester for soft tissue characterization, Biomed. Phys. Eng. Express. 9 (2023), https://doi.org/10.1088/2057-1976/acb940.
[26] H. Xiao, J. Lu, H. Qiu, Y. Li, The range forecast model of traffic incidents impact on urban expressway, Harbin Gongye Daxue Xuebao/Journal Harbin Inst. Technol. 48 (2016) 54–59, https://doi.org/10.11918/j.issn.0367-6234.2016.09.010.
[27] W. Fan, Y. Wang, S. Cai, Fatigue fracture of a highly stretchable acrylic elastomer, Polym. Test. 61 (2017) 373–377, https://doi.org/10.1016/j.polymertesting.2017.06.005.
[28] M. Wu, L. Yang, Q. Shen, Z. Zheng, C. Xu, Endeavour to balance mechanical properties and self-healing of nature rubber by increasing covalent crosslinks via a controlled vulcanization, Eur. Polym. J. 161 (2021), 110823, https://doi.org/10.1016/j.eurpolymj.2021.110823.
[29] M. Englert, F. Minister, A. Moussaoui, W. Pisula, Mechanical properties of thermo-oxidative aged silicone rubber thermally stabilized by titanium oxide based fillers, Polym. Test. 115 (2022), 107726, https://doi.org/10.1016/j.polymertesting.2022.107726.
[30] Y.I. Dzhezherya, W. Xu, S.V. Cherepov, Y.B. Skirta, V.M. Kalita, A.V. Bodnaruk, N. A. Liedienov, A.V. Pashchenko, I.V. Fesych, B. Liu, G.G. Levchenko, Magnetoactive elastomer based on superparamagnetic nanoparticles with Curie point close to room temperature, Mater. Des. 197 (2021), 109281, https://doi.org/10.1016/j.matdes.2020.109281.
[31] K. Suresh, R. Megavarnan, P. Vengatachalam, S. Krishnamurthy, P. Balakrishnan, A review on the effect of various nano fillers on the mechanical properties and thermal stability of chloroprene rubber composites, Mater. Today Proc. 68 (2022) 2560–2568, https://doi.org/10.1016/j.matpr.2022.09.416.
[32] J. Neethirajan, T.S. Natarajan, S. Wiessner, K. Naskar, A. Das, Tuning the mechanical properties of MgO filled epichlorohydrin elastomer composites through in-situ alteration of filler structure using water as stimulus, Mater, Today Commun 26 (2021), 102116, https://doi.org/10.1016/j.mtcomm.2021.102116.
[33] J. Xu, X. Niu, Z. Yao, Mechanical properties and acoustic emission data analyses of crumb rubber concrete under biaxial compression stress states, Construct. Build. Mater. 298 (2021), 123778, https://doi.org/10.1016/j.conbuildmat.2021.123778.
[34] T.H. Le, T. Chan, Y. Kurokawa, H. Inoue, Numerical simulation of deformation-induced temperature variations of a rubber ball under cyclic compression, Int. J. Solid Struct. 248 (2022), 111664, https://doi.org/10.1016/j.ijsolstr.2022.111664.
[35] R. Plachy, C. Hellmich, F. Arthofer, S. Robin, A. Holzner, S. Scheiner, Hydrostatic compression tests, capillary rheometry tests, and extrusion tests performed on unvulcanized rubber confirm importance of compressibility for die swell — arguments from dimensional analysis, Polym. Test. 101 (2021), 107289, https://doi.org/10.1016/j.polymertesting.2021.107289.
[36] A. Erenchun, B. Blanco, N. Gil-Negrete, B. Wang, L. Kari, Effect of lubrication on the mechanical behavior of magnetorheological elastomers in compression mode, Polym. Test. 111 (2022), 107617, https://doi.org/10.1016/j.polymertesting.2022.107617.
[37] A.M.M.R. Persson, E.L. Hinrichsen, E. Andreassen, On the temperature dependence of the cyclic compression behaviour of a thermoplastic vulcanizate elastomer, Polym. Test. 112 (2022), 107650, https://doi.org/10.1016/j.polymertesting.2022.107650.
[38] L.P. Lim, J.C. Juan, N.M. Huang, L.K. Goh, F.P. Leng, Y.Y. Loh, Effect of graphene oxide particle size on the tensile strength and stability of natural rubber graphene composite, Mater. Sci. Eng. B Solid-State Mater. Adv. Technol. 262 (2020), 114762, https://doi.org/10.1016/j.mseb.2020.114762.
[39] A. Masa, S. Iimori, R. Saito, H. Saito, T. Sakai, A. Kaesaman, N. Lopattananon, Strain-induced crystallization behavior of phenolic resin crosslinked natural rubber/clay nanocomposites, J. Appl. Polym. Sci. 132 (2015), https://doi.org/10.1002/app.42580 n/a-n/a.
[40] T. Jose, G. Moni, S. Salini, A.J. Raju, J.J. George, S.C. George, Multifunctional multi-walled carbon nanotube reinforced natural rubber nanocomposites, Ind. Crops Prod. 105 (2017) 63–73, https://doi.org/10.1016/j.indcrop.2017.04.047.
[41] L. Aliotta, V. Gigante, B. Dal Pont, F. Miketa, M.-B. Coltelli, A. Lazzeri, Tearing fracture of poly(lactic acid) (PLA)/poly(butylene succinate-co-adipate) (PBSA) cast extruded films: effect of the PBSA content, Eng. Fract. Mech. 289 (2023), 109450, https://doi.org/10.1016/j.engfracmech.2023.109450.
[42] S. Kiddell, Y. Kazemi, J. Sorken, H. Naguib, Influence of Flash Graphene on the acoustic, thermal, and mechanical performance of flexible polyurethane foam, Polym. Test. 119 (2023), 107919, https://doi.org/10.1016/j.polymertesting.2022.107919.
[43] Q. Wu, W. jia Ma, Q. Liu, K. Zhao, G. Chen, Dynamic shear modulus and damping ratio of rubber-sand mixtures with a wide range of rubber content, Mater. Today Commun. 27 (2021) 15–18, https://doi.org/10.1016/j.mtcomm.2021.102341.
[44] P. Bernal-Ortega, M.M. Bernal, A. González-Jiménez, P. Posadas, R. Navarro, J. L. Valentín, New insight into structure-property relationships of natural rubber and styrene-butadiene rubber nanocomposites filled with MWCNT, Polymer 201 (2020), https://doi.org/10.1016/j.polymer.2020.122604.
[45] A. Esmaeili, M. Hossain, I. Masters, Comparison of two compounding techniques for carbon nanotubes filled natural rubbers through microscopic and dynamic mechanical characterizations, Mater. Lett. 335 (2023), 133786, https://doi.org/10.1016/j.matlet.2022.133786.
[46] A. Esmaeili, I. Masters, M. Hossain, Results in Materials A novel carbon nanotubes doped natural rubber nanocomposite with balanced dynamic shear properties and energy dissipation for wave energy applications, Results Mater 17 (2023), 100358, https://doi.org/10.1016/j.rinma.2022.100358.
[47] S. Cantournet, R. Desmorat, J. Besson, Mullins effect and cyclic stress softening of filled elastomers by internal sliding and friction thermodynamics model, Int. J. Solid Struct. 46 (2009) 2255–2264, https://doi.org/10.1016/j.ijsolstr.2008.12.025.
[48] L.R.G. Treloar, The elasticity of a network of long-chain molecules. II, Rubber Chem. Technol. 17 (1944) 296–302, https://doi.org/10.5254/1.3546653.
[49] M. Mooney, A theory of large elastic deformation, J. Appl. Phys. 11 (1940) 582–592, https://doi.org/10.1063/1.1712836.
[50] R.S. Rivlin, Large elastic deformations of isotropic materials, Collect. Pap. R.S. Rivlin. 243 (1997) 90–108, https://doi.org/10.1007/978-1-4612-2416-7_8.
[51] O.H. Yeoh, Some forms of the strain energy function for rubber, Rubber Chem. Technol. 66 (1993) 754–771, https://doi.org/10.5254/1.3538343.

[52] R.W. Ogden, Large deformation isotropic elasticity - on the correlation of theory and experiment for incompressible rubberlike solids, Rubber Chem. Technol. 46 (1973) 398–416, https://doi.org/10.5254/1.3542910.

[53] A.N. Gent, A new constitutive relation for rubber, Rubber Chem. Technol. 69 (1996) 59–61, https://doi.org/10.5254/1.3538357.

[54] A. Anssari-Benam, A. Bucchi, A generalised neo-Hookean strain energy function for application to the finite deformation of elastomers, Int. J. Non Lin. Mech. 128 (2021), 103626, https://doi.org/10.1016/j.ijnonlinmec.2020.103626.

[55] A. Anssari-Benam, Large isotropic elastic deformations: on a comprehensive model to correlate the theory and experiments for incompressible rubber-like materials, J. Elasticity 153 (2023) 219–244, https://doi.org/10.1007/s10659-022-09982-5.

[56] M. Hossain, P. Steinmann, in: S.P.A. Bordas, D.S. Balint (Eds.), Chapter Three - Continuum Physics of Materials with Time-dependent Properties: Reviewing the Case of Polymer Curing, Elsevier, 2015, pp. 141–259, https://doi.org/10.1016/bs.aams.2015.10.003.

[57] P. Steinmann, M. Hossain, G. Possart, Hyperelastic models for rubber-like materials: consistent tangent operators and suitability for Treloar's data, Arch. Appl. Mech. 82 (2012) 1183–1217, https://doi.org/10.1007/s00419-012-0610-z.

[58] M. Hossain, P. Steinmann, More hyperelastic models for rubber-like materials: consistent tangent operators and comparative study, J. Mech. Behav. Mater. 22 (2013) 27–50, https://doi.org/10.1515/jmbm-2012-0007.

[59] K. Miller, What Material Tests Are Typically Performed to Calibrate a Hyperelastic Material Model?, 2004. http://www.axelproducts.com/downloads/Tests_Hyperelastic_QA.pdf.

[60] I. Axel, Products, Using Slow Cyclic Loadings to Create Stress Strain Curves for Input into Hyperelastic Curve Fitting Routines, 2001.

[61] I. Axel, Products, Testing and Analysis Correlation, 2018. http://www.axelproducts.com/downloads/Fit_Hyperelastic_Stabilized.pdf.

[62] F. Lo Savio, G. La Rosa, M. Bonfanti, A new theoretical-experimental model deriving from the contactless measurement of the thickness of bulge-tested elastomeric samples, Polym. Test. 87 (2020), 106548, https://doi.org/10.1016/j.polymertesting.2020.106548.

[63] J.Y. Sheng, L.Y. Zhang, B. Li, G.F. Wang, X.Q. Feng, Bulge test method for measuring the hyperelastic parameters of soft membranes, Acta Mech. 228 (2017) 4187–4197, https://doi.org/10.1007/s00707-017-1945-x.

[64] I. Jim Day, GM powertrain kurt miller, Axel Products, equibiaxial stretching of elastomeric sheets, an analytical verification of experimental technique, in: ABAQUS 2000 User's Conf. Proc., Newport, Rhode Island, 2000, pp. 1–6. http://www.axelproducts.com/downloads/BiaxialExtension.pdf.

[65] I. Axel Products, Testing Brief: Compression or Biaxial Extension?, n.d. http://www.axelproducts.com/downloads/CompressionOrBiax.pdf..

[66] M. Jiang, R.L. Sridhar, A.B. Robbins, A.D. Freed, M.R. Moreno, A versatile biaxial testing platform for soft tissues, J. Mech. Behav. Biomed. Mater. 114 (2021), 104144, https://doi.org/10.1016/j.jmbbm.2020.104144.

[67] M. Sasso, G. Palmieri, G. Chiappini, D. Amodio, Characterization of hyperelastic rubber-like materials by biaxial and uniaxial stretching tests based on optical methods, Polym. Test. 27 (2008) 995–1004, https://doi.org/10.1016/j.polymertesting.2008.09.001.

[68] K. Morris, A. Rosenkranz, H. Seibert, L. Ringel, S. Diebels, F.E. Talke, Uniaxial and biaxial testing of 3D printed hyperelastic photopolymers, J. Appl. Polym. Sci. 137 (2020) 1–9, https://doi.org/10.1002/app.48400.

[69] T.T. Mai, Y. Morishita, K. Urayama, Novel features of the Mullins effect in filled elastomers revealed by stretching measurements in various geometries, Soft Matter 13 (2017) 1966–1977, https://doi.org/10.1039/c6sm02833k.

[70] M. Johlitz, S. Diebels, Characterisation of a polymer using biaxial tension tests. Part I: hyperelasticity, Arch. Appl. Mech. 81 (2011) 1333–1349, https://doi.org/10.1007/s00419-010-0480-1.

[71] M.R. Claudia Marano, Roberto Calabro, J Polym Sci B Polym Phys - 2010 - Marano - Effect of Molecular Orientation on the Fracture Behavior of Carbon black-filled.Pdf, 2010, pp. 1509–1515.

[72] V.N. Khiêm, J.B. Le Cam, S. Charlès, M. Itskov, Thermodynamics of strain-induced crystallization in filled natural rubber under uni- and biaxial loadings, Part I: complete energetic characterization and crystallinity evaluation, J. Mech. Phys. Solid. 159 (2022), 104701, https://doi.org/10.1016/j.jmps.2021.104701.

[73] H. Seibert, T. Scheffer, S. Diebels, Biaxial testing of elastomers - experimental setup, measurement and experimental optimisation of specimen's shape, Tech. Mech. 34 (2014) 72–89, https://doi.org/10.24352/UB.OVGU-2017-054.

[74] S. Hartmann, R.R. Gilbert, C. Sguazzo, Basic studies in biaxial tensile tests, GAMM-Mitteilungen 41 (2018) 1–14, https://doi.org/10.1002/gamm.201800004.

[75] K.B. Putra, X. Tian, J. Plott, A. Shih, Biaxial test and hyperelastic material models of silicone elastomer fabricated by extrusion-based additive manufacturing for wearable biomedical devices, J. Mech. Behav. Biomed. Mater. 107 (2020), 103733, https://doi.org/10.1016/j.jmbbm.2020.103733.

[76] L.M. Palacios-Pineda, I.A. Perales-Martínez, M.R. Moreno-Guerra, A. Elías-Zúñiga, An optimum specimen geometry for equibiaxial experimental tests of reinforced magnetorheological elastomers with iron micro- and nanoparticles, Nanomaterials 7 (2017), https://doi.org/10.3390/nano7090254.

[77] Y.M. Luo, T.T. Nguyen, H. Attar, L. Chevalier, F. Lesueur, A new biaxial apparatus for tensile tests on Poly Ethylene Terephthalate optimized specimen at stretch blow molding conditions, Polym. Test. 113 (2022), 107676, https://doi.org/10.1016/j.polymertesting.2022.107676.

[78] S. Dedova, K. Schneider, M. Stommel, G. Heinrich, Dissipative heating, fatigue and fracture behaviour of rubber under multiaxial loading, Adv. Polym. Sci. 286 (2021) 421–443, https://doi.org/10.1007/12_2020_75.

[79] T.T. Mai, T. Matsuda, T. Nakajima, J.P. Gong, K. Urayama, Distinctive characteristics of internal fracture in tough double network hydrogels revealed by various modes of stretching, Macromolecules 51 (2018) 5245–5257, https://doi.org/10.1021/acs.macromol.8b01033.

[80] A. Avanzini, D. Battini, Integrated experimental and numerical comparison of different approaches for planar biaxial testing of a hyperelastic material, Adv. Mater. Sci. Eng. 2016 (2016), https://doi.org/10.1155/2016/6014129.

[81] D. Ahmad, R.M. Ajaj, M. Amoozgar, Elastomer-based skins for morphing aircraft applications: effect of biaxial strain rates and prestretch, Polym. Test. 113 (2022), 107655, https://doi.org/10.1016/j.polymertesting.2022.107655.

[82] Y. Kodaira, T. Miura, Y. Takano, A. Yonezu, Development of biaxial tensile testing for porous polymer membranes, Polym. Test. 106 (2022), 107440, https://doi.org/10.1016/j.polymertesting.2021.107440.

[83] M.N. Silberstein, P.V. Pillai, M.C. Boyce, Biaxial elastic-viscoplastic behavior of Nafion membranes, Polymer 52 (2011) 529–539, https://doi.org/10.1016/j.polymer.2010.11.032.

[84] B. Yohsuke, K. Urayama, T. Takigawa, K. Ito, Biaxial strain testing of extremely soft polymer gels, Soft Matter 7 (2011) 2632–2638, https://doi.org/10.1039/c0sm00955e.

[85] T.T. Mai, K. Urayama, Biaxial loading effects on strain energy release rate and crack-tip strain field in elastic hydrogels, Macromolecules 54 (2021) 4792–4801, https://doi.org/10.1021/acs.macromol.1c00445.

[86] M. Jiang, J. Dai, G. Dong, Z. Wang, A comparative study of invariant-based hyperelastic models for silicone elastomers under biaxial deformation with the virtual fields method, J. Mech. Behav. Biomed. Mater. 136 (2022), 105522, https://doi.org/10.1016/j.jmbbm.2022.105522.

[87] X. Zhao, Z.C. Berwick, J.F. Krieger, H. Chen, S. Chambers, G.S. Kassab, Novel design of cruciform specimens for planar biaxial testing of soft materials, Exp. Mech. 54 (2014) 343–356, https://doi.org/10.1007/s11340-013-9808-4.

[88] A. Makinde, L. Thibodeau, K.W. Neale, Development of an apparatus for biaxial testing using cruciform specimens, Exp. Mech. 32 (1992) 138–144, https://doi.org/10.1007/BF02324725.

[89] S. Demmerle, J.P. Boehler, Optimal design of biaxial tensile cruciform specimens, J. Mech. Phys. Solid. 41 (1993) 143–181, https://doi.org/10.1016/0022-5096(93)90067-P.

[90] A. Smits, D. Van Hemelrijck, T.P. Philippidis, A. Cardon, Design of a cruciform specimen for biaxial testing of fibre reinforced composite laminates, Compos. Sci. Technol. 66 (2006) 964–975, https://doi.org/10.1016/j.compscitech.2005.08.011.

[91] E. Lamkanfi, W. Van Paepegem, J. Degrieck, Shape optimization of a cruciform geometry for biaxial testing of polymers, Polym. Test. 41 (2015) 7–16, https://doi.org/10.1016/j.polymertesting.2014.09.016.

[92] A. Makris, T. Vandenbergh, C. Ramault, D. Van Hemelrijck, E. Lamkanfi, W. Van Paepegem, Shape optimisation of a biaxially loaded cruciform specimen, Polym. Test. 29 (2010) 216–223, https://doi.org/10.1016/j.polymertesting.2009.11.004.

[93] R. Ranjan, H. Murthy, D. Bhowmik, V.S. Sadavarte, Behaviour of composite solid propellant under biaxial tensile loading, Polym. Test. 124 (2023), 108054, https://doi.org/10.1016/j.polymertesting.2023.108054.

[94] I. Erukhimovich, M.O. de la Cruz, Effect of molecular orientation on the fracture behavior of carbon black-filled, Nat. Rubber Comp. 48 (2004) 1509–1515, https://doi.org/10.1002/polb.

[95] G. Schubert, P. Harrison, Equi-biaxial tension tests on magneto-rheological elastomers, Smart Mater. Struct. 25 (2015), https://doi.org/10.1088/0964-1726/25/1/015015.

[96] H.K.S. Kawabata, M. Matsuda Matsuda, K. Tei, Experimental survey of the strain energy density function of isoprene rubber vulcanizate, Macromolecules 14 (1981) 154–162.

[97] T. Kawamura, K. Urayama, S. Kohjiya, Multiaxial deformations of end-linked poly (dimethylsiloxane) networks 5. Revisit to mooney-rivlin approach to strain energy density function, Nihon Reoroji Gakkaishi 31 (2003) 213–217, https://doi.org/10.1678/rheology.31.213.

[98] S. Saikrasun, S. Bualek-Limcharoen, S. Kohjiya, K. Urayama, Anisotropic mechanical properties of thermoplastic elastomers in situ reinforced with thermotropic liquid-crystalline polymer fibers revealed by biaxial deformations, J. Polym. Sci., Part B: Polym. Phys. 43 (2005) 135–144, https://doi.org/10.1002/polb.20315.

[99] J. Schmidtke, S. Kniesel, H. Finkelmann, Probing the photonic properties of a cholesteric elastomer under biaxial stress, Macromolecules 38 (2005) 1357–1363, https://doi.org/10.1021/ma0487655.

[100] A. Helal, M. Doumit, R. Shaheen, Biaxial experimental and analytical characterization of a dielectric elastomer, Appl. Phys. Mater. Sci. Process 124 (2018) 1–11, https://doi.org/10.1007/s00339-017-1422-3.

[101] D. Jalocha, A. Constantinescu, R. Nevière, Prestrained biaxial DMA investigation of viscoelastic nonlinearities in highly filled elastomers, Polym. Test. 42 (2015) 37–44, https://doi.org/10.1016/j.polymertesting.2015.01.005.

[102] A. Azoug, A. Thorin, R. Nevière, R.M. Pradeilles-Duval, A. Constantinescu, Influence of orthogonal prestrain on the viscoelastic behaviour of highly-filled elastomers, Polym. Test. 32 (2013) 375–384, https://doi.org/10.1016/j.polymertesting.2012.12.005.

[103] X. Chen, L. Meng, W. Zhang, K. Ye, C. Xie, D. Wang, W. Chen, M. Nan, S. Wang, L. Li, Frustrating strain-induced crystallization of natural rubber with biaxial stretch, ACS Appl. Mater. Interfaces 11 (2019) 47535–47544, https://doi.org/10.1021/acsami.9b15865.

[104] D. Ahmad, S.K. Sahu, K. Patra, Fracture toughness, hysteresis and stretchability of dielectric elastomers under equibiaxial and biaxial loading, Polym. Test. 79 (2019), 106038, https://doi.org/10.1016/j.polymertesting.2019.106038.
[105] D. Ahmad, R.M. Ajaj, Multiaxial mechanical characterization of latex skin for morphing wing application, Polym. Test. 106 (2022), 107408, https://doi.org/10.1016/j.polymertesting.2021.107408.
[106] D. Xiang, X. Chen, J. Li, Y. Wu, C. Zhao, H. Li, Z. Li, L. Wang, P. Wang, Y. Li, J. Wang, Flexible strain sensors with high sensitivity and large working range prepared from biaxially stretched carbon nanotubes/polyolefin elastomer nanocomposites, J. Appl. Polym. Sci. 140 (2023) 1–12, https://doi.org/10.1002/app.53371.
[107] O.K. Garishin, V.V. Shadrin, Y.V. Kornev, Mechanical studies of rubber micro- and nanocomposites promising for the tire industry. Uniaxial and biaxial tests, Mater. Phys. Mech. 42 (2019) 445–454, https://doi.org/10.18720/MPM.4242019_9.
[108] Y. Xue, P. Ravishankar, M.A. Zeballos, V. Sant, K. Balachandran, S. Sant, Valve leaflet-inspired elastomeric scaffolds with tunable and anisotropic mechanical properties, Polym. Adv. Technol. 31 (2020) 94–106, https://doi.org/10.1002/pat.4750.
[109] M. Ru, X.Q. Lei, X.M. Liu, Y.J. Wei, An equal-biaxial test device for large deformation in cruciform specimens, Exp. Mech. 62 (2022) 677–683, https://doi.org/10.1007/s11340-021-00810-w.
[110] P. Hu, J. Madsen, A.L. Skov, One reaction to make highly stretchable or extremely soft silicone elastomers from easily available materials, Nat. Commun. 13 (2022) 1–10, https://doi.org/10.1038/s41467-022-28015-2.
[111] J.J. Hu, G.W. Chen, Y.C. Liu, S.S. Hsu, Influence of specimen geometry on the estimation of the planar biaxial mechanical properties of cruciform specimens, Exp. Mech. 54 (2014) 615–631, https://doi.org/10.1007/s11340-013-9826-2.
[112] M. Fujikawa, N. Maeda, J. Yamabe, Y. Kodama, M. Koishi, Determining stress–strain in rubber with in-plane biaxial tensile tester, Exp. Mech. 54 (2014) 1639–1649, https://doi.org/10.1007/s11340-014-9942-7.
[113] M. Brieu, J. Diani, N. Bhatnagar, A new biaxial tension test fixture for uniaxial testing machine - a validation for hyperelastic behavior of rubber-like materials, J. Test. Eval. 35 (2007) 364–372, https://doi.org/10.1520/jte100688.
[114] H. Hariharaputhiran, U. Saravanan, A new set of biaxial and uniaxial experiments on vulcanized rubber and attempts at modeling it using classical hyperelastic models, Mech. Mater. 92 (2016) 211–222, https://doi.org/10.1016/j.mechmat.2015.09.003.
[115] F. Zhang, Z. Fan, X. Du, Z. Kuang, Study on viscoelastic properties of cord-rubber composite subjected to biaxial loading, J. Elastomers Plast. 36 (2004) 143–156, https://doi.org/10.1177/0095244304041757.
[116] F. Caimmi, R. Calabrò, F. Briatico-Vangosa, C. Marano, M. Rink, Toughness of natural rubber compounds under biaxial loading, Eng. Fract. Mech. 149 (2015) 250–261, https://doi.org/10.1016/j.engfracmech.2015.08.003.
[117] J. Lavazza, M. Contino, C. Marano, Strain rate, temperature and deformation state effect on Ecoflex 00-50 silicone mechanical behaviour, Mech. Mater. 178 (2023), 104560, https://doi.org/10.1016/j.mechmat.2023.104560.
[118] A. Corti, T. Shameen, S. Sharma, A. De Paolis, L. Cardoso, Biaxial testing system for characterization of mechanical and rupture properties of small samples, HardwareX 12 (2022), e00333, https://doi.org/10.1016/j.ohx.2022.e00333.
[119] T. Aoyama, N. Yamada, K. Urayama, Nonlinear elasticity of ultrasoft near-critical gels with extremely sparse network structures revealed by biaxial stretching, Macromolecules 54 (2021) 2353–2365, https://doi.org/10.1021/acs.macromol.0c02737.
[120] X. Gao, E. Sözümert, Z. Shi, G. Yang, V.V. Silberschmidt, Mechanical modification of bacterial cellulose hydrogel under biaxial cyclic tension, Mech. Mater. 142 (2020), 103272, https://doi.org/10.1016/j.mechmat.2019.103272.
[121] T.T. Mai, T. Matsuda, T. Nakajima, J.P. Gong, K. Urayama, Damage cross-effect and anisotropy in tough double network hydrogels revealed by biaxial stretching, Soft Matter 15 (2019) 3719–3722, https://doi.org/10.1039/c9sm00409b.
[122] Y. Bin, Y. Tanabe, C. Nakabayashi, H. Kurosu, M. Matsuo, Morphology and mechanical properties of swollen gels and dry gel films of poly(vinyl alcohol) prepared by crystallization from solutions under simultaneous biaxially stretching, Polymer 42 (2001) 1183–1200, https://doi.org/10.1016/S0032-3861(00)00423-7.
[123] M. Fujine, T. Takigawa, K. Urayama, Strain-driven swelling and accompanying stress reduction in polymer gels under biaxial stretching, Macromolecules 48 (2015) 3622–3628, https://doi.org/10.1021/acs.macromol.5b00642.
[124] T. Katashima, K. Urayama, U. Il Chung, T. Sakai, Strain energy density function of a near-ideal polymer network estimated by biaxial deformation of Tetra-PEG gel, Soft Matter 8 (2012) 8217–8222, https://doi.org/10.1039/c2sm25340b.
[125] Y. Kondo, K. Urayama, M. Kidowaki, K. Mayumi, T. Takigawa, K. Ito, Applicability of a particularly simple model to nonlinear elasticity of slide-ring gels with movable cross-links as revealed by unequal biaxial deformation, J. Chem. Phys. 141 (2014), https://doi.org/10.1063/1.4897134.
[126] C. Zhang, X. Gou, R. Xiao, Hysteresis in glass microsphere filled elastomers under cyclic loading, Polym. Test. 95 (2021), 107081, https://doi.org/10.1016/j.polymertesting.2021.107081.
[127] H. Attar, Y.M. Luo, L. Chevalier, T.T. Nguyen, F. Detrez, Identification of anisotropic properties of polymer sheets from heterogeneous biaxial tests, Polym. Test. 115 (2022), 107721, https://doi.org/10.1016/j.polymertesting.2022.107721.
[128] Z. Wang, N. Boechler, S. Cai, Anisotropic mechanical behavior of 3D printed liquid crystal elastomer, Addit. Manuf. 52 (2022), 102678, https://doi.org/10.1016/j.addma.2022.102678.
[129] D. Pearce, M. Nemcek, C. Witzenburg, Combining unique planar biaxial testing with full-field thickness and displacement measurement for spatial characterization of soft tissues, Curr. Protoc. 2 (2022), https://doi.org/10.1002/cpz1.493.
[130] M. Ahmadi, A. Shojaei, Reinforcing mechanisms of carbon nanotubes and high structure carbon black in natural rubber/styrene-butadiene rubber blend prepared by mechanical mixing-effect of bound rubber, Polym. Int. 64 (2015) 1627–1638, https://doi.org/10.1002/pi.4964.
[131] S. Dedova, K. Schneider, M. Stommel, G. Heinrich, Dissipative heating, fatigue and fracture behaviour of rubber under multiaxial loading, in: Adv. Polym. Sci., Springer Science and Business Media Deutschland GmbH, 2021, pp. 421–443, https://doi.org/10.1007/12_2020_75.
[132] Biaxial testing System for high static and dynamic Loading of Discover more interesting articles and news on the subject Entdecken Sie weitere interessante Artikel und News zum Thema, 2018.
[133] B. Dong, L. Zhang, Y. Wu, Influences of different dimensional carbon-based nanofillers on fracture and fatigue resistance of natural rubber composites, Polym. Test. 63 (2017) 281–288, https://doi.org/10.1016/j.polymertesting.2017.08.035.
[134] Y. Zhou, S. Jerrams, A. Betts, L. Chen, Fatigue life prediction of magnetorheological elastomers subjected to dynamic equi-biaxial cyclic loading, Mater. Chem. Phys. 146 (2014) 487–492, https://doi.org/10.1016/j.matchemphys.2014.03.059.
[135] Y. Zhou, S. Jerrams, L. Chen, Multi-axial fatigue in magnetorheological elastomers using bubble inflation, Mater. Des. 50 (2013) 68–71, https://doi.org/10.1016/j.matdes.2013.02.071.
[136] R. Kaltseis, C. Keplinger, S.J. Adrian Koh, R. Baumgartner, Y.F. Goh, W.H. Ng, A. Kogler, A. Tröls, C.C. Foo, Z. Suo, S. Bauer, Natural rubber for sustainable high-power electrical energy generation, RSC Adv. 4 (2014) 27905–27913, https://doi.org/10.1039/c4ra03090g.
[137] Z. Xu, S. Jerrams, H. Guo, Y. Zhou, L. Jiang, Y. Gao, L. Zhang, L. Liu, S. Wen, Influence of graphene oxide and carbon nanotubes on the fatigue properties of silica/styrene-butadiene rubber composites under uniaxial and multiaxial cyclic loading, Int. J. Fatig. 131 (2020), 105388, https://doi.org/10.1016/j.ijfatigue.2019.105388.
[138] M. Johnson, N. Murphy, R. Ekins, J. Hanley, S. Jerrams, Equi-biaxial fatigue testing of EPM utilising bubble inflation, Polym. Test. 53 (2016) 122–131, https://doi.org/10.1016/j.polymertesting.2016.05.017.
[139] Y. Zhou, L. Jiang, S. Chen, J. Ma, A. Betts, S. Jerrams, Determination of reliable fatigue life predictors for magnetorheological elastomers under dynamic equi-biaxial loading, Polym. Test. 61 (2017) 177–184, https://doi.org/10.1016/j.polymertesting.2017.05.021.
[140] K. Kojio, A. Fujimoto, T. Kajiwara, C. Nagano, S. Masuda, C.H. Cheng, S. Nozaki, K. Kamitani, H. Watanabe, A. Takahara, Advantages of bulge testing and rupture mechanism of glassy polymer films, Polymer 179 (2019), 121632, https://doi.org/10.1016/j.polymer.2019.121632.
[141] U.D. Çakmak, I. Kallaí, Z. Major, Temperature dependent bulge test for elastomers, Mech. Res. Commun. 60 (2014) 27–32, https://doi.org/10.1016/j.mechrescom.2014.05.006.
[142] G. Machado, D. Favier, G. Chagnon, Membrane curvatures and stress-strain full fields of axisymmetric bulge tests from 3D-DIC measurements. Theory and validation on virtual and experimental results, Exp. Mech. 52 (2012) 865–880, https://doi.org/10.1007/s11340-011-9571-3.
[143] L.R.G. Treloar, Strains in an inflated rubber sheet, and the mechanism of bursting, Rubber Chem. Technol. 17 (1944) 957–967, https://doi.org/10.5254/1.3546716.
[144] C.E. Miller, J.P. Lavery, T.A. Donnelly, Determination of elastic parameters for human fetal membranes, J. Rheol. 23 (1979) 57–78, https://doi.org/10.1122/1.549534.
[145] P. Seshaiyer, F.P.K. Hsu, A.D. Shah, S.K. Kyriacou, J.D. Humphrey*, Multiaxial mechanical behavior of human saccular aneurysms, Comput. Methods Biomech. Biomed. Eng. 4 (2001) 281–289, https://doi.org/10.1080/10255840108908009.
[146] A. Anssari-Benam, A. Bucchi, G. Saccomandi, Modelling the Inflation and Elastic Instabilities of Rubber-like Spherical and Cylindrical Shells Using a New Generalised Neo-Hookean Strain Energy Function, 2022, https://doi.org/10.1007/s10659-021-09823-x. The Author(s).
[147] A. Anssari-Benam, Comparative modelling results between a separable and a non-separable form of principal stretches–based strain energy functions for a variety of isotropic incompressible soft solids: Ogden model compared with a parent model, Mech. Soft Mater. 5 (2023), https://doi.org/10.1007/s42558-023-00050-z.
[148] I. Standard, INTERNATIONAL STANDARD Metallic Materials — Sheet and Strip —, 2003, p. 2003.
[149] A. Chretien, M. Daigle, A. Hacker, B. Rinkel, Design of a Biaxial Test Device to Measure Soft Tissue Properties, 2018.
[150] L. Pini, Geometry Optimization for Biaxial Testing of Polydimethylsiloxane SYLGARD 184 and Finite Element Modelling, 2020, pp. 1–107. http://hdl.handle.net/10589/154541.